

This manuscript has been accepted for publication in the AIAA Journal. Please cite this manuscript as:
Zhao, W. and Kapania, R. K., "Prestressed Vibration of Stiffened Variable Angle Tow Laminated Plates,"
AIAA Journal, 2019, DOI: 10.2514/1.J057719

Prestressed Vibration of Stiffened Variable Angle Tow Laminated Plates

Wei Zhao* and Rakesh K. Kapania†

Virginia Polytechnic Institute and State University, Blacksburg, VA, 24061

Compared to straight fiber path laminates, variable angle tow (VAT) laminates are known to redistribute the in-plane stress resultants for improving structural buckling response. The VAT laminates can also be used to improve the free vibration response by tailoring the structural elastic stiffness. This paper studies the prestressed vibration response of a stiffened, VAT laminated plate under a uniform end-shortening. Because there are both spatially dependent stiffener and fiber path orientations for a stiffened, VAT laminated plate, a separate modeling of the plate and stiffeners is considered. This method avoids placing common nodes at stiffener-plate and stiffener-stiffener interfaces. This allows one to study mesh convergence for the plate and the stiffeners, separately. It also improves the efficiency and robustness of the finite element model. The finite element code based on the present method is verified extensively using examples, that are either available in literature or are analyzed using commercial software. Parametric studies show that, depending on the in-plane load and boundary condition, the VAT laminates with linearly varying (LV) fiber paths can increase the prestressed vibration fundamental frequency when compared to the straight fiber path laminates. Optimization studies found that using nonlinearly varying (NLV) fiber paths, when compared to the LV fiber paths, causes a significant increase in the buckling load but only a slight increase in the case of free or prestressed vibration fundamental frequencies. The VAT laminates appear to mainly tailor the panel's elastic stiffness for improving the prestressed vibration response for the stiffened plates with clamped edges. However, for the simply-supported stiffened plate, the

*Post-doctoral Fellow, Kevin T. Crofton Department of Aerospace and Ocean Engineering, weizhao@vt.edu, AIAA Member

†Norris and Wendy Mitchell Endowed Professor, Kevin T. Crofton Department of Aerospace and Ocean Engineering, rkapania@vt.edu, AIAA Associate Fellow

VAT laminates are mainly used to change both the elastic and geometric stiffness matrices for improving the prestressed vibration response.

Nomenclature

A_s	=	stiffener cross-sectional area, m ²
a	=	length of the composite panel, m
\mathbf{B}	=	displacement-strain matrix
b	=	width of the composite panel, m
b_s	=	width of the composite stiffener, m
\mathbf{D}	=	constitutive matrix giving stress resultant-strain relations
d_p	=	panel displacements
d_s	=	stiffener displacements described in a local coordinate system
d_{sg}	=	stiffener displacements described in a global coordinate system
e	=	eccentricity of a stiffener, $e = \frac{1}{2} (t_p + h_s)$
E_1, E_2	=	Young's modulus along principal 1-axis and 2-axis, respectively, Pa
h_s	=	stiffener height, m
I_n, I_b	=	stiffener second moment of area about the n and b axis, respectively, m ⁴
J_s	=	effective polar area moment of inertia for orthotropic beams, m ⁴
\mathbf{J}	=	Jacobian of the coordinate transformation
K_{cr}	=	normalized buckling parameter
\mathbf{K}_p	=	panel elastic stiffness matrix
\mathbf{K}_s	=	stiffener elastic stiffness matrix
\mathbf{K}_{Gp}	=	panel geometric stiffness matrix
\mathbf{K}_{Gs}	=	stiffener geometric stiffness matrix
\mathbf{M}_p	=	panel mass matrix
\mathbf{M}_s	=	stiffener mass matrix
\mathbf{N}_{sp}	=	shape functions to approximate stiffener nodal displacement and geometry
N_{xx}, N_{yy}, N_{xy}	=	in-plane stress resultants, N/m

P_{cr}	=	the critical buckling load for the laminated plate, N
\mathbf{r}	=	vector for geometry field, $r = (x, y)$
\mathbf{T}_s	=	transformation matrix for stiffener displacement
t_p	=	panel thickness, m
t, n, b	=	stiffener tangential, normal and binormal directions, respectively
w	=	transverse displacement, m
Γ	=	stiffener arch length domain
Θ	=	a vector for fiber path angles at reference points for each layer
θ_0, θ_1	=	variable fiber path angles at normalized location of $\bar{x} = 0$ and $ \bar{x} = 1$, respectively, degrees
λ_b	=	eigenvalue from buckling analysis, <i>i.e.</i> , buckling load factor
λ_v	=	eigenvalue from free vibration analysis
$\bar{\lambda}_v$	=	normalized eigenvalue from free vibration analysis
ξ, η	=	natural coordinates for plate element
ζ	=	natural coordinate for beam element
σ^0	=	external in-plane stress vector, Pa
ε, σ	=	strain and stress, respectively
β	=	plate's rotational angle, radian
ω_c	=	natural circular frequency, radian/s
$\bar{\omega}$	=	normalized fundamental frequency
Ω	=	panel area domain
Subscripts		
cr	=	critical value
p	=	plate
s	=	stiffener
t	=	total model, <i>i.e.</i> , stiffened plate
Abbreviations		
LV	=	linearly varying
NLV	=	nonlinearly varying

QI	=	quasi-isotropic
SF	=	straight fiber

I. Introduction

Dynamic response generated during normal operations for aerospace vehicles under complex load conditions, such as gust, acoustic, or other dynamic loads, can lead to fatigue problems. The resonance or near-resonance structural vibration amplitude can influence the aircraft normal operation and reduce the structure and surrounding electronic components' life [1]. The in-plane loads for a wing/fuselage panel, such as the compressive force generated at the aircraft wing upper skin panels during cruising, could lead to a reduction in the panel's transverse stiffness, which can reduce the panel's fundamental frequency and increase the transient vibration amplitude under external random loads and lead to fatigue and even to panel flutter. Several approaches were considered for improving structural dynamic responses including adding constraints for the vibration frequencies [2] and the undamped vibration amplitude (or transient responses) [3], and minimization of the resonance amplitude using passive damping for specific modes [4].

Applications of integrated, bonded, and stitched stiffened composite structures have been considered in aerospace structural design due to their higher specific strength-to-weight and specific stiffness-to-weight ratios [5, 6] and their tailorability for improving the structural dynamic responses [7–9]. Recent advances in novel manufacturing technologies, such as automated fiber placement (AFP) machines and repeatable placement of pre-preg composite tows using computer-aided-engineering [10], have made it possible to fabricate composite laminates with spatially-varying angle fiber plies. Research has shown that such composite structures with variable-angle-tow (VAT) laminates can improve the structural performance including strength, buckling and free vibration responses as compared to plates that use straight fiber path laminated composites [11, 12]. The VAT laminates are mainly found to redistribute the panel's in-plane stress resultants to improve the buckling responses under various in-plane loads [11], while the stiffeners are mainly used to modify the buckling/vibration mode shape wavelengths [13] to improve the corresponding responses. It is of great interest to combine these two functionalities for improving the prestressed vibration response of a stiffened composite plate in the presence of the in-plane axial loads/end-shortening.

Structural analysis of VAT laminated panels for studying their strength and buckling responses has received considerable research interest during last several decades. Hyer and Charette [14] found that the curvilinear fiber path for composite structures has a potential for a further improvement in the structural

performance of composites as compared to that with straight fiber path. Gürdal and Olmedo [11] conducted a detailed stress analysis study on a VAT laminated plate subjected to an in-plane load and concluded that it is possible to use the VAT laminates to tailor the stress resultants distribution to further improve the structural performance, as compared to that of using straight fiber path laminates. Wu *et al.* [15, 16] conducted both numerical and experimental studies on VAT laminated plates and showed an increased load-carrying capability of the VAT laminated panels over traditional straight fiber path laminates. Lopes *et al.* [17, 18] found that it is the load-redistribution capacity of a VAT laminated plate that increases its buckling load and delays the initiation of damage and final structural failure. Coburn *et al.* [19] have also studied the benefit of using VAT laminates for improving the buckling of stiffened, VAT laminated plates. Since then, a lot of research efforts have been made towards the structural analysis and optimization of the VAT laminated plates to improve their structural static strength, buckling and postbuckling responses [19–22].

As compared to the static and buckling analyses of VAT laminated structures, there are very few works available on vibration analysis of such composite structures [23]. The first work on dynamic analysis of a VAT laminated plate appears to have been conducted by Abdalla *et al.* [12], who studied the fundamental frequency maximization for the VAT laminated plate using lamination parameters. Research studies showed that using VAT laminates can increase the fundamental frequency for composite plates at different plate aspect ratios, boundary conditions and material orthotropy degrees. Additionally, Blom *et al.* [24] studied the fundamental frequency maximization for a variable-stiffness conical shell and found that the VAT laminates can increase the fundamental frequency as compared to that of using straight fiber path laminates even while considering manufacturing constraints.

Honda *et al.* [25, 26] presented an analytical method for studying free vibration mode results of a laminated plate with curvilinear fibers using the Ritz method. A B-spline based parameterization is used to parameterize the fiber paths for the VAT laminates. Different plate aspect ratios and boundary conditions were considered for studying the variations in both the natural frequencies and mode shapes with respect to the VAT fiber path angles [26]. In addition to increasing the fundamental frequency by using VAT laminates, the fiber paths in VAT laminates also affect the mode shapes for higher modes. The optimization studies show that the VAT laminates lead to little or no improvement in the fundamental frequency for the plate with a simply-supported boundary condition, but it can increase the fundamental frequency for the plate with clamped edge(s). The optimal fiber paths were oriented to be or close to be perpendicular to the clamped edge(s) to increase the free vibration fundamental frequency [25].

Akhavan and Ribeiro [27] presented a new p -version finite element along with a third-order shear de-

formation theory (TSDT) for studying natural vibration modes of a rectangular VAT laminated plate. A linearly varying (LV) fiber path angle and manufacturing constraints in fabricating such fiber paths were considered in the vibration analysis. Parametric studies were conducted on the free vibration natural frequencies for the VAT laminated plate by varying the fiber path angles. Both vibration modal frequencies and mode shapes can be tailored by using VAT laminates. Free vibration mode shapes for higher modes can be tailored to change the natural frequencies to improve the dynamic response. The first vibration mode shapes for different VAT laminates were found to be close to each other when the boundary conditions are same. The computational results agreed well with the experimental data for both the modal frequencies and the corresponding mode shapes [28, 29].

To investigate the influence of the geometric nonlinearity on vibration responses of a VAT laminated plate, nonlinear vibration responses have been also studied. Ribeiro and Akhavan [30] studied the transient dynamic responses using a new p -version finite element method with hierarchic basis functions based on the first-order shear deformation theory and considered the geometric nonlinearity for modeling the VAT laminated plate. Ribeiro [31] used a similar method as presented in Ref. [30] to study the nonlinear free periodic vibrations of VAT laminated plates. Both works showed that VAT laminates can, depending on the external load, decrease the oscillation amplitude as compared to that using constant-stiffness laminates.

In addition to the free and forced vibration response studies for the VAT laminates, aeroelastic response for a VAT laminated plate was also studied. Stodieck *et al.* [32] used the Rayleigh-Ritz approach to study flutter of a tow-steered composite plate. A cantilever plate model similar to a wing was considered and research studies showed that the VAT laminates can improve the panel flutter speed by up to 14% as compared to that using standard UD laminate. Stanford *et al.* [33] conducted aeroelastic tailoring for a cantilever VAT laminated plate for optimal performance in stress and flutter boundary using a genetic algorithm. As compared to the optimal straight fiber path laminates, optimal tow-steering laminate can either increase the flutter boundary or reduce the stress but not both simultaneously. Guimarães *et al.* [34] studied the panel flutter of plates with VAT laminates. Optimization studies showed that VAT laminate fiber path angles parameterized using a high-order Lagrange polynomial can increase the flutter speed by up to 20.5% as compared to that of using straight fiber path laminates. Akhavan and Ribeiro [35] also studied the panel flutter for a VAT laminated structure with different boundary conditions and concluded that the advantage of using VAT laminates for improving the flutter speed is boundary condition dependent.

The VAT laminates are mainly used to redistribute the in-plane stress resultants and to improve the bending stiffness, respectively, for improving the buckling responses for the plate under end-shortening and

for maximizing the plate's free fundamental natural frequency. Also, the stiffeners can alter the mode shapes for improving both buckling and vibration responses for the stiffened plates. These motivate us to study the prestressed vibration responses for stiffened, VAT laminated plates under in-plane end-shortening in the present work. Furthermore, to the best of the authors' knowledge and also based on a recent review on VAT laminates work [23], there is no available research work on vibration analysis of both unstiffened and stiffened, VAT laminated plate under in-plane loads or end shortening. Hence, the present work can provide guidelines towards using stiffened, VAT laminates for structural design of practical composite structures in the presence of complex boundary conditions, while also providing benchmarks for vibration analysis of both unstiffened and stiffened, VAT laminated plates.

The paper is organized as follows: Section II presents the expressions of the strain energy, kinetic energy, and the external work for a stiffened, VAT laminated plate for performing prestressed vibration analysis. The stiffener displacement and geometry approximations and all matrices used in an eigenvalue computation for prestressed vibration modal results are presented in this section. Sections III and IV present detailed verification studies on buckling, free and prestressed vibration analysis of both unstiffened and stiffened, VAT laminated plates, respectively. Section V presents results from parametric studies on investigating the effect of LV fiber path angles on the stiffened plate's prestressed vibration responses with different boundary conditions. Optimization studies on using NLV fiber path laminates for improving the stiffened plate's buckling, free and prestressed vibration responses are conducted in Section VI. The last section, Section VII, concludes the work.

II. Relevant Formulations

A. Strain Energy, Kinetic Energy and External Work

The approach presented in this work models the stiffener and the VAT laminated plate separately for a stiffened plate. The plate and the stiffener are, respectively, modeled by using the flat shell and composite beam elements based on Mindlin plate and Timoshenko beam theories. The displacement compatibility conditions at the plate-stiffener interfaces are considered so that the stiffener's displacement and geometry can be approximated in terms of those for the plate. A local coordinate system, tnb , is used to describe the generalized stiffener's motion. A detailed study using this approach for structural analysis of a stiffened composite plate with straight fiber path laminates has been presented in our previous works [9, 13], which will not be shown here for brevity. However, for completeness, the expressions for the required energies

needed for deriving the governing equations for a prestressed vibration analysis are briefly presented.

The strain energy, U_t , for the stiffened, VAT composite panel is obtained by summing them for the plate, U_p , and the stiffeners, U_s as:

$$U_t = U_p + U_s \quad (1a)$$

$$U_p = \frac{1}{2} \iint_{\Omega} \{\mathbf{d}_p\}^T [\mathbf{B}_p]^T [\mathbf{D}_p]^T [\mathbf{B}_p] \{\mathbf{d}_p\} d\Omega \quad (1b)$$

$$U_s = \frac{1}{2} \int_{\Gamma} \{\boldsymbol{\varepsilon}_s\}^T [\mathbf{D}_s]^T \{\boldsymbol{\varepsilon}_s\} d\Gamma = \frac{1}{2} \int_{\Gamma} \{\mathbf{d}_p\}^T [\mathbf{N}_{sp}]^T [\mathbf{T}_s]^T [\mathbf{B}_s]^T [\mathbf{D}_s] [\mathbf{B}_s] [\mathbf{T}_s] [\mathbf{N}_{sp}] \{\mathbf{d}_p\} d\Gamma \quad (1c)$$

where $\{\mathbf{d}_p\}$ is the generalized displacement field for the point at the middle surface of a composite panel and $[\mathbf{B}_p]$ is the strain-displacement relation matrix for the panel. The stiffener path is denoted as Γ . The matrix $[\mathbf{T}_s]$ is a transformation matrix which relates the stiffener displacement field, $\{\mathbf{d}_s\}$, described in the local coordinate system *tnb* and the stiffener displacement field, $\{\mathbf{d}_{sg}\}$, described in the global coordinate system *xyz*, $\{\mathbf{d}_s\} = [\mathbf{T}_s]\{\mathbf{d}_{sg}\}$. Matrices $[\mathbf{B}_s]$ and $[\mathbf{D}_s]$ are the displacement-strain matrix and the stress resultant-strain constitutive matrix, respectively, for the stiffener. The expression for those matrices are not shown here for brevity, all of which can be found in Ref. [13]. The transformation matrix $[\mathbf{N}_{sp}]$ is used to approximate the stiffener displacement in terms of the plate displacement based on the finite element shape functions for the isoparametric eight-noded shell elements, which is briefly shown in Section II-B.

Similarly, for buckling analysis, the external work, W_t , for the stiffened plate can be obtained by summing the work, W_p , of the panel due to the in-plane stress resultants, $\{\boldsymbol{\sigma}^0\}$, and the work for the stiffener, W_s , in the presence of an axial stress, σ_t , and is given as:

$$W_t = W_p + W_s \quad (2a)$$

$$W_p = \iiint_V \{\boldsymbol{\sigma}^0\}^T \{\boldsymbol{\varepsilon}_p^{NL}\} dV = \frac{1}{2} \iint_{\Omega} [\mathbf{d}_p]^T [\mathbf{B}_p^{NL}]^T [\boldsymbol{\sigma}_p] [\mathbf{B}_p^{NL}] \{\mathbf{d}_p\} d\Omega \quad (2b)$$

$$W_s = \frac{1}{2} \int_{\Gamma} \{\mathbf{d}_p\}^T [\mathbf{N}_{sp}]^T [\mathbf{T}_s]^T [\mathbf{B}_s^{NL}]^T [\boldsymbol{\sigma}_s] [\mathbf{B}_s^{NL}] [\mathbf{T}_s] [\mathbf{N}_{sp}] \{\mathbf{d}_p\} d\Gamma \quad (2c)$$

where $\{\boldsymbol{\varepsilon}_p^{NL}\}$ is a vector for the nonlinear terms of the in-plane strains obtained through Green-Lagrange strain tensor. The in-plane stress resultants vector, $\{\boldsymbol{\sigma}^0\}$, among the panel can be obtained from the residual stress, the external applied load, and the initial displacement constraints, etc. In the present work, we consider an in-plane end-shortening for computing the in-plane stress resultants. The stiffener axial stress resultant matrix is $[\boldsymbol{\sigma}_s]$ and the stiffener geometric stiffness relation matrix is $[\mathbf{B}_s^{NL}]$. The expression for these matrices and vectors can be found in Ref. [13].

The kinetic energy, T_t , of the stiffened composite panel is expressed as:

$$T_t = T_p + T_s \quad (3a)$$

$$T_p = \frac{1}{2} \iint_{\Omega} \left\{ \dot{\mathbf{d}}_p \right\}^T [\mathbf{m}_p] \left\{ \dot{\mathbf{d}}_p \right\} d\Omega \quad (3b)$$

$$T_s = \frac{1}{2} \int_{\Gamma} \left\{ \dot{\mathbf{d}}_p \right\}^T [\mathbf{N}_{sp}]^T [\mathbf{T}_s]^T [\mathbf{m}_s] [\mathbf{T}_s] [\mathbf{N}_{sp}] \left\{ \dot{\mathbf{d}}_p \right\} d\Gamma \quad (3c)$$

where $[\mathbf{m}_p]$ is mass matrix per area for the plate and $[\mathbf{m}_s]$ is the mass matrix per length for the stiffener [13].

The (\cdot) represents the first-order derivative with respect to time.

B. Stiffener displacement approximation

The method on modeling the stiffeners and plate separately in this paper was studied in detail in our previous work [9]. For completeness, we briefly present the approach to compute the matrix \mathbf{N}_{sp} . The transformation matrix \mathbf{N}_{sp} is used to approximate the stiffener displacement and geometry fields in terms of the plate displacement components using the finite element shape functions for the isoparametric elements.

The stiffness and mass matrices for the stiffeners can be transformed to those for the plate.

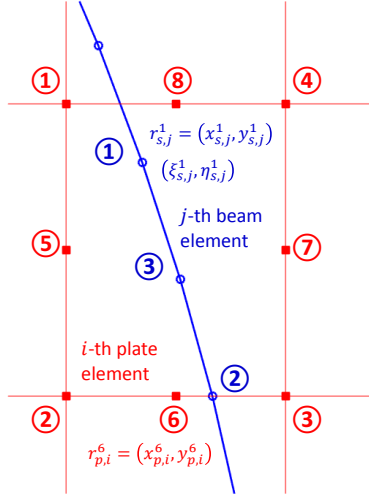


Figure 1: Approximation of stiffener beam element nodal displacement in term of those for the plate element

Figure 1 shows the j -th beam element, which is used to model the stiffener, passing through the i -th plate element. Both the displacement and geometry expressions for the node of the j -th beam element can be approximated in terms of those for the eight nodes of the i -th plate element based on the isoparametric elements used in the finite element method. Hence, the nodal displacement and the geometry for each node

($m = 1, 2, 3$) of the j -th beam element can be expressed as:

$$d_{sg,j}^m = \sum_{k=1}^8 N_{p,i}^k(\xi_{s,j}^m, \eta_{s,j}^m) d_{p,i}^k, \quad r_{s,j}^m = \sum_{k=1}^8 N_{p,i}^k(\xi_{s,j}^m, \eta_{s,j}^m) r_{p,i}^k \quad (4)$$

where N_p is the shape function for an eight-noded shell element, $(\xi_{s,j}^m, \eta_{s,j}^m)$ are natural coordinates for the m -th node of the j -th beam element within the i -th plate element as shown in Fig. 1. The symbol i for the plate element is not shown in Eq. (4). Since the geometry fields for the plate $\{\mathbf{r}_p\}$ and the stiffeners $\{\mathbf{r}_s\}$ are known, the natural coordinates $(\xi_{s,j}^m, \eta_{s,j}^m)$ can be obtained through the geometric approximations for isoparametric elements. The natural coordinates are then used to approximate the stiffener displacements. Hence, all nodal displacements for the stiffeners can be obtained and written in a matrix form as:

$$\{\mathbf{d}_{sg}\} = [\mathbf{N}_{sp}]\{\mathbf{d}_p\} \quad (5)$$

The stiffener displacement field described in the global coordinate system, $\{\mathbf{d}_{sg}\}$, can be transformed to that described in the stiffener local coordinate system using a transformation matrix, $[\mathbf{T}_s]$.

C. Finite Element Analysis

For a linear prestressed vibration analysis studied here, the procedure is to perform a pre-buckling analysis to obtain the stress distribution in both the panel and the stiffeners. The geometric stiffness for both the plate and the stiffeners are computed in terms of the obtained stress distribution. The stress distribution is obtained in terms of an in-plane end-shortening, $\{\Delta\mathbf{d}\}$. The linear static analysis equation is given as:

$$([\mathbf{K}_p] + [\mathbf{K}_s])\{\mathbf{d}_p\} = \{\mathbf{F}\} \quad (6)$$

Equation 6 can be solved based on the end-shortening, $\{\Delta\mathbf{d}\}$ in $\{\mathbf{d}_p\}$. Once the deflection $\{\mathbf{d}_p\}$ is obtained, the stress components for both the plate and the stiffeners can be computed, respectively, as:

$$\{\boldsymbol{\sigma}_p\} = [\mathbf{Q}_p]\{\boldsymbol{\varepsilon}_p\} = [\mathbf{Q}_p][\mathbf{B}_p]\{\mathbf{d}_p\}, \quad \{\boldsymbol{\sigma}_t\} = [\mathbf{Q}_s]\{\boldsymbol{\varepsilon}_t\} = [\mathbf{Q}_s][\mathbf{B}_s][\mathbf{T}_s][\mathbf{N}_{sp}]\{\mathbf{d}_p\} \quad (7)$$

where $[\mathbf{Q}_p]$ and $[\mathbf{Q}_s]$ are the in-plane stress-strain relations for the plate and the stiffener, respectively; the strains $\{\boldsymbol{\varepsilon}_p\}$ and $\{\boldsymbol{\varepsilon}_t\}$ have different values computed at different Gauss integration points for each element in the VAT laminates. There are 3×3 and three Gaussian integration points considered for the plate and the stiffener, respectively. In this work, the in-plane strains for the plate, $\{\boldsymbol{\varepsilon}_p\}$, and the stiffeners, $\{\boldsymbol{\varepsilon}_t\}$, are obtained by averaging the strain components that are computed at Gauss integration points:

$$\{\boldsymbol{\varepsilon}_p\} = \frac{1}{9} \sum_{k=1}^9 [\mathbf{B}_p(\xi_k, \eta_k)] \{\mathbf{d}_p\}, \quad \{\boldsymbol{\varepsilon}_t\} = \frac{1}{3} \sum_{k=1}^3 [\mathbf{B}_s(\zeta_k)] [\mathbf{T}_s] [\mathbf{N}_{sp}] \{\mathbf{d}_p\} \quad (8)$$

An eigenvalue analysis is conducted using the following equation to obtain the buckling load factor, λ_b :

$$(([K_p] + [K_s]) + \lambda_b ([K_{Gp}] + [K_{Gs}])) \{\mathbf{u}_p\} = \{\mathbf{0}\} \quad (9)$$

where the buckling load factor, λ_b , and the corresponding buckling mode shape, $\{\mathbf{u}_p\}$, can be obtained by performing an eigenvalue analysis.

Finally, the governing equations for a vibration analysis of the stiffened composite panel in the presence of the in-plane stress is given as:

$$(([K_p] + [K_s]) + w_0 \lambda_b ([K_{Gp}] + [K_{Gs}]) - \omega^2 ([M_p] + [M_s])) \{\mathbf{d}_p\} = \{\mathbf{0}\} \quad (10)$$

where the load factor $w_0 \in [0, 1]$. When $w_0 = 0$, the above equation is for a free vibration analysis and when $w_0 = 1$, the stiffened plate buckles and the first vibration modal frequency is zero.

The element stiffness matrices, $[K_p^e]$ and $[K_s^e]$, the element geometric stiffness matrices, $[K_{Gp}^e]$ and $[K_{Gs}^e]$ and the element mass matrices, $[M_p^e]$ and $[M_s^e]$, for the stiffened composite panel, respectively, are:

$$\begin{aligned} K_p^e &= \int_{-1}^{+1} \int_{-1}^{+1} [\mathbf{B}_p]^T [\mathbf{D}_p]^T [\mathbf{B}_p] \det[\mathbf{J}_p] d\xi d\eta \quad K_s^e = \int_{-1}^{+1} [\mathbf{N}_{sp}]^T [\mathbf{T}_s]^T [\mathbf{B}_s]^T [\mathbf{D}_s]^T [\mathbf{B}_s] [\mathbf{T}_s] [\mathbf{N}_{sp}] \det \mathbf{J}_s d\xi \\ K_{Gp}^e &= \int_{-1}^{+1} \int_{-1}^{+1} [\mathbf{B}_p^{NL}]^T [\boldsymbol{\sigma}_p] [\mathbf{B}_p^{NL}] \det[\mathbf{J}_p] d\xi d\eta, \quad K_{Gs}^e = \int_{-1}^{+1} [\mathbf{N}_{sp}]^T [\mathbf{T}_s]^T [\mathbf{B}_s^{NL}]^T [\boldsymbol{\sigma}_s] [\mathbf{B}_s^{NL}] [\mathbf{T}_s] [\mathbf{N}_{sp}] \det \mathbf{J}_s d\xi \\ M_p^e &= \int_{-1}^{+1} \int_{-1}^{+1} [\mathbf{m}_p] \det[\mathbf{J}_p] d\xi d\eta, \quad M_s^e = \int_{-1}^{+1} [\mathbf{N}_{sp}]^T [\mathbf{T}_s]^T [\mathbf{m}_s] [\mathbf{T}_s] [\mathbf{N}_{sp}] \det \mathbf{J}_s d\xi \end{aligned} \quad (11)$$

where $[\mathbf{J}_p]$ and $[\mathbf{J}_s]$ are the Jacobians for the panel and the stiffener, along with other matrices, all of them can be found in Ref. [13].

It should be pointed out that when evaluating VAT laminated plate element stiffness matrices, $[K_p^e]$ and $[K_{Gp}^e]$, Gaussian quadrature may not give highly accurate results for those matrices. This is because both the rigidity matrix, $[\mathbf{D}_p]$ and stress matrix for the plate, $[\boldsymbol{\sigma}_p]$ are highly spatial dependent. Hao *et al.* [36] evaluated the elemental stiffness for the VAT laminate plate where the fiber orientation for each layer is evaluated at Gaussian integration points. This integration approach may not be highly accurate as the spatial dependent stiffness rigidity matrix leading to a change in the polynomial order or evaluation fitness function not being a polynomial anymore.

Numerical integration methods, such as the quasi-Monte Carlo method, can be used but such a method is very expensive as it might require a large number of random sample points for converged results. Alterna-

tively, one can use a constant fiber path angle evaluated at the element center for each layer for computing $[\mathbf{K}_p^e]$ and $[\mathbf{K}_{Gp}^e]$ when using Gaussian quadrature. This integration method would require a very fine mesh that is used for a VAT laminated plate with nonlinear fiber paths. Our research has shown that using a mesh (24×24), for an unstiffened square plate with LV fiber path laminates [37], can lead to converged and accurate results, within 1% of analytical results. For nonlinearly varying (NLV) fiber path laminates, such as a Lagrange polynomial based fiber path angles [20], a slightly fine mesh for the unstiffened square VAT laminated plate (32×32) using the present method still give converged and accurate results around 1%.

Note that the manufacturing constraints on fiber path, such as the fiber path curvature radius constraint, are not considered at this time. The density of VAT laminated plate is assumed to be independent of the fiber path orientation. A general framework for different shaped fiber paths for the plate is developed in the present work.

D. Variable Angle Tow Laminates

Different methods are available for parameterizing the fiber path angles, such as a linear variation based fiber path orientation [11, 38, 39], the Lagrange polynomials based nonlinear fiber orientations [20], and a B-spline based expression [25, 40], among others. Lamination parameters have also been widely used to describe the local stiffness properties using a finite set of continuous design variables in structural optimization [41, 42]. A post-processing is required to determine the actual fiber angle distribution when using the optimal lamination parameters, e.g., using a curve fitting technique [43]. Wu *et al.* [20] found that using Lagrange polynomials to parameterize the fiber path angle may achieve the optimal buckling load close to that obtained using lamination parameters. Therefore, the present work uses Lagrange polynomials to parameterize the fiber path angle as shown in Eq. (12). The fiber path orientation is defined in a quarter of the square plate, which is same as that used by Wu *et al.* [20] and is shown in Fig. 2. The laminate configuration is defined as $[\pm\Theta_1, \pm\Theta_2]_s$, where $\Theta_1 = [\theta_{mn}]_1$ and $\Theta_2 = [\theta_{mn}]_2$. Here θ_{mn} is the fiber path angle at the reference point, $r_{mn} = (x_m, y_n)$.

$$\theta(x, y) = \sum_{m=0}^{M-1} \sum_{n=0}^{N-1} \theta_{mn} \cdot \prod_{i \neq m} \left(\frac{x - x_i}{x_m - x_i} \right) \cdot \prod_{j \neq n} \left(\frac{y - y_j}{y_n - y_j} \right) \quad (12)$$

When there are two reference points, Eq. (12) becomes a LV fiber path. The LV fiber path is normally denoted as $\langle \theta_0 | \theta_1 \rangle$ where θ_0 and θ_1 are defined at the plate's center and edges, respectively. The reference points, (x_m, y_n) , can have any arbitrary distribution. In the present work, uniformly distributed reference points are considered. Representative fiber paths for each layer are shown in Fig. 3 where the reference

angles at the 9 reference points as used by Wu *et al.* [20] are given in Appendix A.

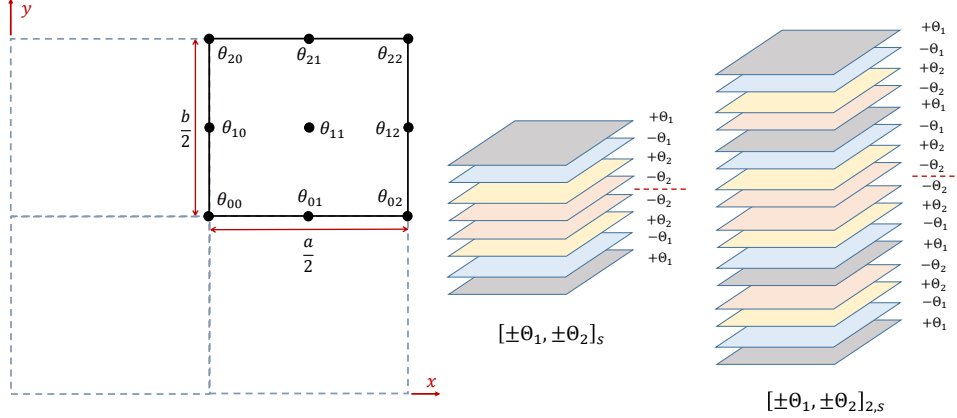


Figure 2: Parameterization of VAT fiber path orientation using Lagrange Polynomials [20]

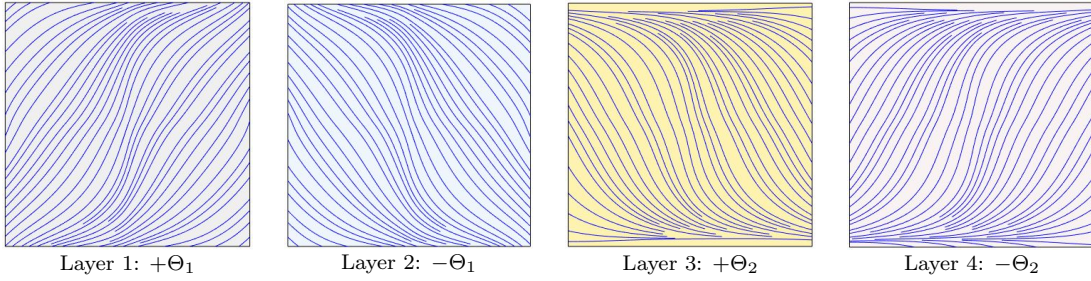


Figure 3: Representative nonlinear fiber paths for each layer; Matlab command `streamslice` is used to plot fiber path; note that the line drop in the plot does not mean the fiber drop in this study

III. Verification Studies of Unstiffened VAT Laminates

For a linearly prestressed vibration analysis, all matrices as given in Eq. (10) are needed to be verified. This section first verifies the present program in conducting buckling, free and prestressed vibration of unstiffened, VAT laminated plate using available results in literature.

A. Natural vibration of a free rectangular VAT laminated plate

A rectangular VAT laminated plate with dimensions of 0.4 m (length) \times 0.3 m (width) studied by Rodrigues *et al.* [28, 29] is used to verify the present program on computing the free vibration mode results. A free boundary condition is considered. The material properties and laminate configurations are not shown here for brevity, which can be found in Rodrigues *et al.* [28].

Table 1 shows both mesh convergence and validation studies in free vibration modal frequencies. Note

Table 1: Mesh convergence and validation studies for free vibration modal frequencies of VAT laminated plate with free boundary conditions (unit: Hz)

Mode ¹	12 × 9	16 × 12	24 × 18 ²	32 × 24	40 × 30	NASTRAN	TSDT [29]	FEM [28]	Experimental tests [28]
1	47.84	47.85	47.88	47.89	47.89	47.91 (-0.06%)	48.06 (-0.37%)	47.13 (1.59%)	50.90 (-5.93%)
2	50.27	50.26	50.25	50.25	50.25	50.22 (0.05%)	50.37 (-0.24%)	49.45 (1.62%)	57.52 (-12.64%)
3	85.84	85.78	85.74	85.73	85.72	85.71 (0.03%)	85.95 (-0.24%)	84.28 (1.73%)	85.78 (-0.05%)
4	107.79	107.77	107.81	107.81	107.81	107.82 (-0.01%)	108.24 (-0.40%)	106.16 (1.55%)	109.28 (-1.35%)
5	117.37	117.37	117.35	117.36	117.36	117.37 (-0.02%)	117.87 (-0.44%)	115.65 (1.47%)	120.14 (-2.32%)
6	161.56	161.37	161.41	161.47	161.49	161.44 (-0.02%)	161.88 (-0.29%)	159.40 (1.26%)	162.36 (-0.59%)
7	202.16	202.09	202.10	202.13	202.15	202.14 (-0.02%)	203.01 (-0.45%)	199.34 (1.38%)	195.64 (3.30%)

¹ The mode number means the elastic mode

² The difference in bracket () using the present method computed at a mesh size of 24×18

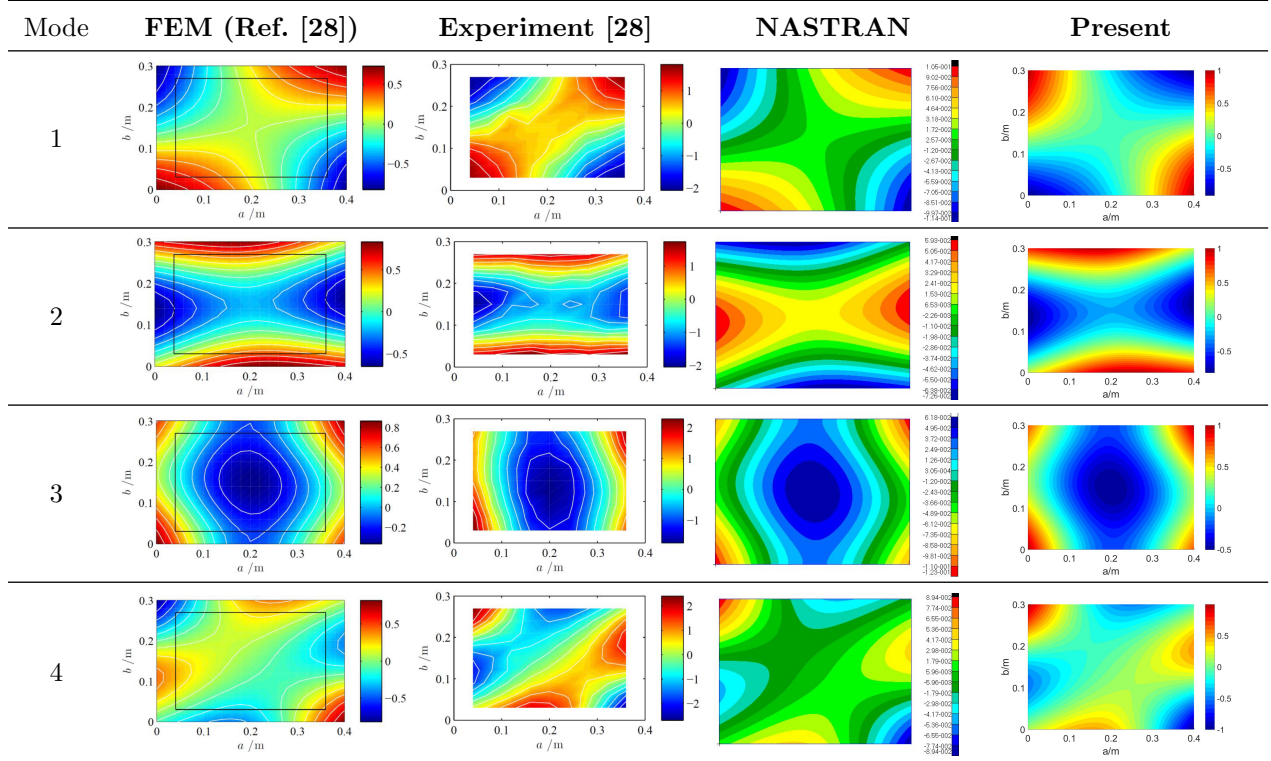


Figure 4: Comparisons of the first 4 mode shapes for a free rectangular VAT laminated plate

that the mesh size not only influences the convergence of the results just as is the case for a laminated plate with straight fibers, but it also affects the fiber ply orientation for each layer for the case of the VAT laminates. The converged free vibration frequency values match very well with the available results [28, 29].

Experimental data is also available for this case. The second modal frequency, however, does not correlate well with the test data for all analytical/numerical results. The authors in Ref. [28] explained the discrepancy by stating that the excitation point selected during ground vibration test does not sufficiently excite the 2nd mode. Hence, as another independent check, a free vibration modal analysis for this model is also conducted using a commercially available FEA package, MSC NASTRAN. A four-noded quadrilateral plate element, CQUAD4, is employed to model the plate. A relatively fine mesh of 120×100 elements for the complete plate is used to ensure that the converged results are obtained. For each layer, each element has a constant fiber path angle evaluated at its center. The present results also show a good agreement with those obtained using NASTRAN. The first four free vibration mode shapes obtained from different sources show an excellent agreement as shown in Fig. 4. Note that the present results used for comparison purposes are obtained by using a mesh size of 24×18 for the VAT laminated plate. The comparisons of the first 7 elastic mode shapes can be found in the supplemental material in Section 1.1 of [Supp_Data.pdf](#).

B. Natural vibration of a clamped square VAT laminated plate

A fully clamped square VAT laminated plate studied by Ribeiro and Akhavan [30] is employed to further validate the present program for studying free vibration of a VAT laminated plate. For brevity, the geometry and laminate configurations are not shown here. The mesh size for the square plate is 24×24 . The first four elastic modal frequencies that change with the ply orientation, θ_1 , and with a fixed center fiber ply orientation, $\theta_0 = 45^\circ$, are shown in Fig. 5.

It is observed that the frequencies for all fiber ply orientations computed using the present method are in an excellent agreement with the available data. It is also found that, as compared to the laminate configuration with straight fibers, $[\pm 45|45]_{2,s}$, it is possible to further improve the fundamental frequency by using the VAT laminates. The data for modal frequencies given in Fig. 5 can be found in the supplemental material in Section 1.2 of [Supp_Data.pdf](#).

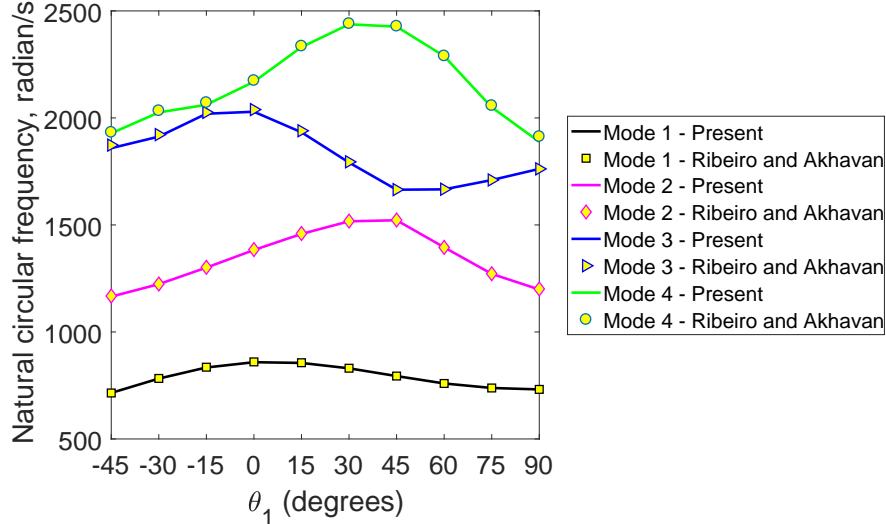


Figure 5: Variation of natural circular frequency with fiber ply orientation, $[\pm 45|\theta_1]_{2,s}$

C. Buckling of a VAT laminated plate

A simply-supported square VAT laminated plate with side dimension of $a = b = 0.254$ m subjected to a uniform end-shortening along the x -axis, Δu , used by Wu *et al.* [20] is considered. The convergence and verification studies for the buckling coefficient computed using the present program are shown in Table 2. For brevity, the fiber path orientations for the three cases (c)-(e) are not shown here. These can be found in Ref. [20].

Table 2: Mesh convergence and verification studies of the normalized buckling coefficient, K_{cr} , of a VAT laminated plate

Case	Fiber path	8×8	16×16	24×24	<u>32×32</u>	48×48	Wu <i>et al.</i> [20]	Diff.
(a)	$[0 \pm 45 0]_{2s}$	1.08	1.06	1.08	1.08	1.08	1.08 (1.07) ¹	-0.20% (0.73%) ²
(b)	$[90 \pm 0 75]_{2s}$	2.77	2.91	2.94	2.95	2.96	2.98 (2.97)	-1.01% (-0.67%)
(c)	#1 NLV(y) ²	3.28	3.43	3.45	3.46	3.47	3.50 (3.50)	-1.14% (-1.14%)
(d)	#2 NLV(x, y) ²	3.44	3.61	3.64	3.65	3.66	3.71 (3.68)	-1.62% (-0.54%)
(e)	#3 NLV(x, y) ²	3.55	3.66	3.70	3.71	3.71	3.78 (3.73)	-1.85% (-0.54%)

¹: The values shown in bracket by Wu *et al.* [20] were obtained using ABAQUS

²: The percentages shown in the bracket are compared against results obtained by Wu *et al.* [20] using ABAQUS

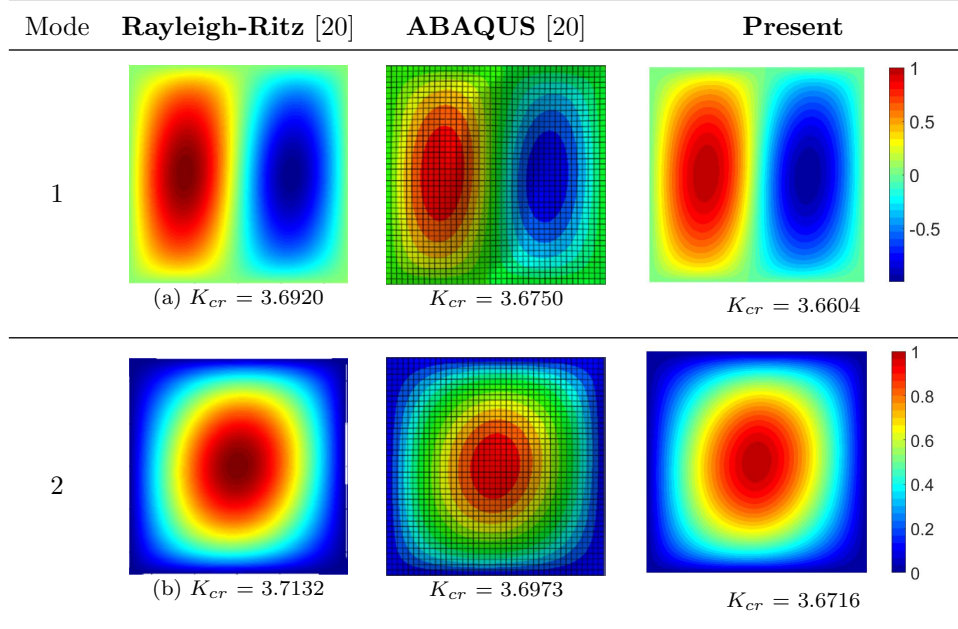


Figure 6: Comparisons of first two buckling modes for case (d) given in Table 2

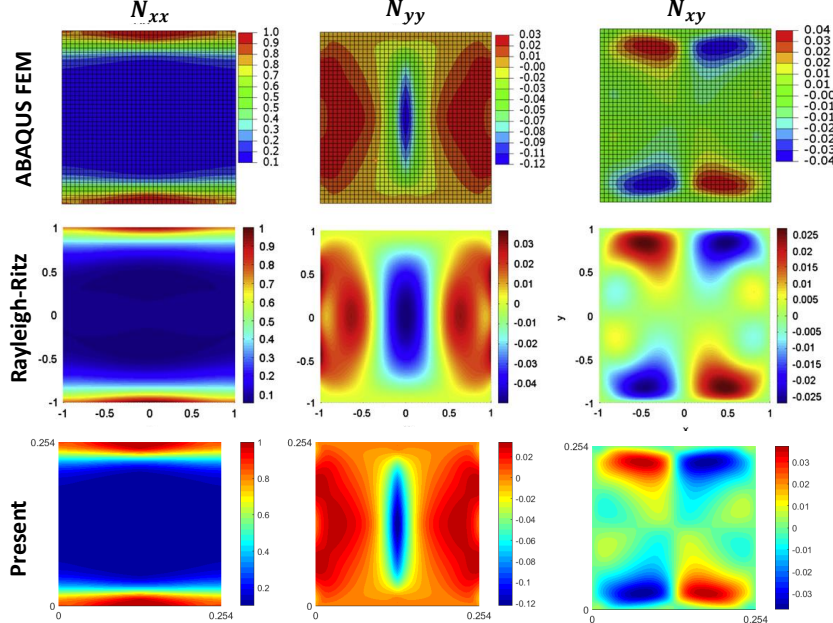


Figure 7: Comparisons of in-plane stress resultants distribution for the case (d)

The buckling load is obtained as $P_{cr} = \lambda_b \int_{-b/2}^{b/2} N_{xx}(a/2, y) dy$ where N_{xx} is the in-plane stress resultant (N/m) and λ_b is the buckling load factor obtained from a buckling eigenvalue computation. The normalized buckling coefficient is defined as $K_{cr} = \frac{P_{cr}a^2}{E_1bt_p^3}$. Table 2 show that the buckling load converges well with the

mesh size for the plate with various fiber path laminates. The buckling loads and the corresponding buckling mode shapes (see Fig. 6) computed using the present program for all cases are in a good agreement with those computed by Wu *et al.* [20].

The stress resultants for N_{xx} , N_{yy} and N_{xy} are normalized with respect to the maximum value, $N_{xx,max}$, as shown in Fig. 7. In the present results, $N_{xx,max} = 6.37E4$ (N/m). The present stress resultants' distribution matches well with those obtained by using Rayleigh-Ritz approach and ABAQUS FEM [20]. The stress resultants values, N_{yy} and N_{xy} , are much less than those of N_{xx} . It is noticed that the maximum in-plane axial stress resultants (N_{xx}) are shifted to the panel's edge for improving the buckling response.

D. Prestressed vibration of a VAT laminated plate

A simply-supported square VAT laminated plate studied by Samukham *et al.* [44] is used to verify the present program on the prestressed vibration of a VAT laminated plate. A uniform end-shortening, Δu , is considered. A prestressed vibration is studied for the VAT laminates in the presence of the in-plane compression up to the buckling load. A normalized fundamental frequency is computed, which is defined as $\bar{\omega} = \frac{\omega a^2 \sqrt{\rho/E_2}}{h}$ where ω is the modal natural frequency (Hz).

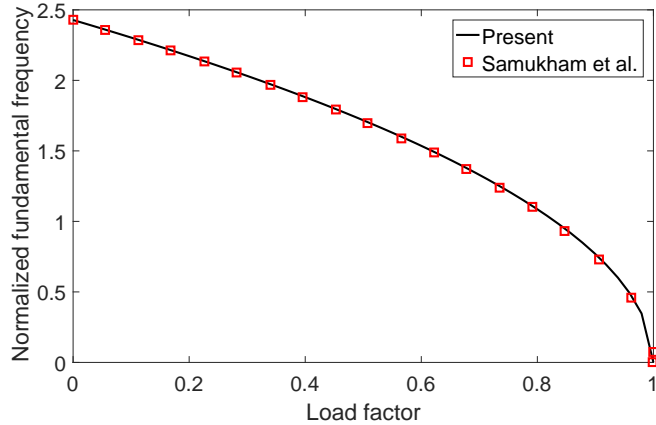


Figure 8: Variation of the normalized fundamental frequency with the applied load factor, $[\pm(0|30)]_{3,s}$

For a simply-supported plate with VAT laminate configurations of $[\pm(0|30)]_{3,s}$, the normalized fundamental frequency and the normalized buckling load factor are, $\bar{\omega} = 2.428$ (2.429) and $K_{cr} = 1.33$ (1.37), respectively. The values in the bracket are obtained by Samukham *et al.* [44]. Figure 8 shows the normalized fundamental frequency for the VAT laminated plate with the in-plane load up to the buckling load. The present results, obtained using a mesh size of 24×24 for the square plate, match well with those obtained by Samukham *et al.* [44]. The discrete points data in the plot are extracted using Webplotdigitizer [45].

IV. Verification Studies of Buckling and Prestressed Vibration of Stiffened VAT Laminates

This section mainly focuses on verification studies for prestressed vibration analysis of a stiffened, VAT laminated plate subjected to an in-plane end-shortening. Based on our previous work [13] on free and prestressed vibration of stiffened composite plates with straight-fiber laminated plate and the free vibration studies for the unstiffened, VAT laminates in the previous Section III, we can conclude that the present program can accurately compute the free vibration responses of the stiffened, VAT laminates. Since there appear to be no available results in literature regarding prestressed vibration analysis of the stiffened, VAT laminates, a NASTRAN model is employed to verify the present program on studying the prestressed vibration of stiffened, VAT laminated plates. In this verification section, the configuration of the laminate is $[\pm\Theta_1, \pm\Theta_2]_{2,s}$ as given in Fig. 2 where Θ_1 and Θ_2 are given in Appendix A.

A. Two Straight Equidistant Stiffeners

A simply-supported square laminated wing skin panel [46] with dimensions of $0.30m \times 0.30m$ is considered. Two straight equidistant blade stiffeners, placed at $y = b/3$ and $y = 2b/3$, as shown in Fig. 9a are considered. The stiffener depth ratio is fixed to $h_s/b_s = 5$ for global buckling and free vibration studies, which is less than that (7.5) studied by Coburn *et al.* [19]. On the other hand, stiffener may buckle in its lateral direction with a depth ratio larger than 10 [13]. The stiffener width, b_s , equals the panel thickness, t_p . The material properties for both the laminated plate and the composite stiffeners are same and are given as: $E_1 = 181$ GPa, $E_2 = 10.27$ GPa, $G_{12} = 7.17$ GPa, $G_{13} = G_{23} = 4$ GPa, $\nu_{12} = 0.28$ and density $\rho = 1800$ kg/m³. The layer thickness is 1.272×10^{-4} m.

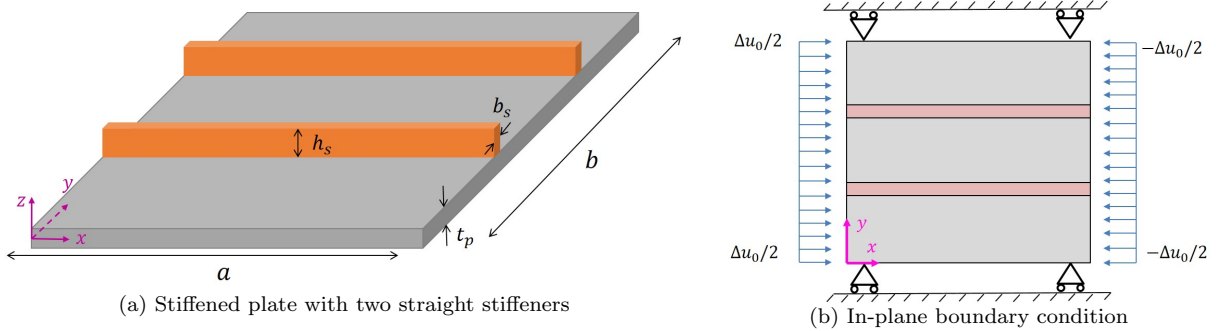


Figure 9: A square VAT laminated panel with two straight stiffeners and in-plane boundary condition

Consider a uniform end-shortening on the panel edges, Δu_0 (see Fig. 9b), used in the verification study.

The four edges of the panel are simply-supported as they are attached to the internal spars and ribs for a wing box. For the pre-buckling analysis, (a) $x = 0, u_0 = \frac{\Delta u_0}{2}$; (b) $x = a, u_0 = -\frac{\Delta u_0}{2}$, (c) $y = (0, b), v_0 = 0$ and (d) $w = 0$ for four edges.

To show the benefit of the present method in modeling the stiffeners and the plate separately, we first conduct a mesh convergence study for performing the plate's buckling and prestressed vibration analysis. The converged mesh for the plate with NLV fiber path laminates, 32×32 , is used in the subsequent prestressed vibration analysis for the stiffened plates. Both concentric and eccentric stiffeners are considered for the stiffened plate in the buckling and prestressed vibration verification studies. A fine mesh size of 100×100 is used for the plate and 100 beam elements for each stiffener are considered in an analysis using NASTRAN for obtaining converged results for subsequent comparisons. The composite stiffeners are modeled as orthotropic beams, which are equivalent to the laminated stiffeners with zero straight fiber path angle.

Results from the convergence studies on prestressed vibration responses with respect to the number of stiffener beam elements are presented in Table 3. Doubling the stiffener beam elements from 20 to 40, all modal frequencies undergo less than a 0.5% change. Hence, the results for the stiffened plate computed with 20 beam elements for each stiffener are considered to be converged. It is clearly observed that the present converged results match well with NASTRAN results. The first two buckling and prestressed vibration mode shapes for both concentric and eccentric stiffener cases are shown in Fig. 10. They are in a good agreement with the NASTRAN results. The NASTRAN input files for the model are given in Appendix C. Results also show that for the stiffened, VAT laminated plate, one can use a fewer number of elements in the present method to model stiffeners when using a slightly fine mesh for the plate with NLV fiber path laminates.

B. Curvilinear Stiffeners

As mentioned in the previous section, the present method allows one to model the stiffeners and the VAT laminated plate separately. To further demonstrate this capability, we also verify the present program for studying the prestressed vibration of a stiffened, VAT laminated plate with arbitrarily shaped stiffeners. Four curvilinear stiffeners, generated using the approach presented in previous work [37], are considered. The geometric model of the stiffened plate is shown in Fig. 11a. The physical coordinates for the four stiffeners are also given in Appendix B. The NASTRAN mesh and the present mesh are shown in Figs. 11b and 11c, respectively. Note that the fine mesh in NASTRAN is normally used by EBF3PanelOpt [47] to avoid meshing failure. Triangle elements (CTRIA3) are used in NASTRAN model for the plate. The fiber path angle for each layer is evaluated at each triangle element center for the NASTRAN model.

Table 3: Mesh convergence and verification studies of prestressed modal frequencies, ω (unit: Hz), of stiffened NLV fiber path laminated plate with respect to stiffener elements number under a uniform end-shortening, $\Delta u_0 = 2 \times 10^{-5}$ m

Mode	Concentric stiffeners, $e = 0$						Eccentric stiffeners, $e \neq 0$					
	5	10	20	40	NASTRAN	Diff.	5	10	20	40	NASTRAN	Diff.
1	181.93	182.15	182.59	182.65	183.82	-0.67%	328.16	330.64	335.37	336.03	332.86	0.76%
2	327.87	327.95	328.14	328.17	329.19	-0.32%	402.29	403.64	406.29	406.67	407.32	-0.25%
3	585.76	589.39	595.13	595.99	598.23	-0.52%	599.24	599.32	599.48	599.52	600.23	-0.12%
4	597.35	597.37	597.41	597.43	609.67	-2.01%	790.89	793.69	796.69	797.09	795.00	0.21%
5	668.68	670.59	673.75	674.23	682.10	-1.22%	791.29	797.11	804.92	806.07	804.22	0.09%
6	818.26	818.40	818.61	818.69	819.50	-0.11%	897.92	912.82	934.31	937.66	915.18	2.09%
7	978.89	979.02	979.09	979.11	980.42	-0.14%	1019.10	1019.73	1021.32	1022.65	1021.18	-0.13%
8	1075.18	1090.89	1107.75	1110.14	1140.20	-2.85%	1170.91	1171.81	1172.49	1172.64	1173.03	-0.05%
9	1118.70	1125.45	1132.76	1133.82	1147.70	-1.30%	1192.45	1202.98	1212.06	1213.31	1214.95	-0.24%
10	1181.16	1182.07	1183.54	1183.90	1189.78	-0.53%	1301.11	1336.17	1367.55	1371.97	1367.55	0.08%

21

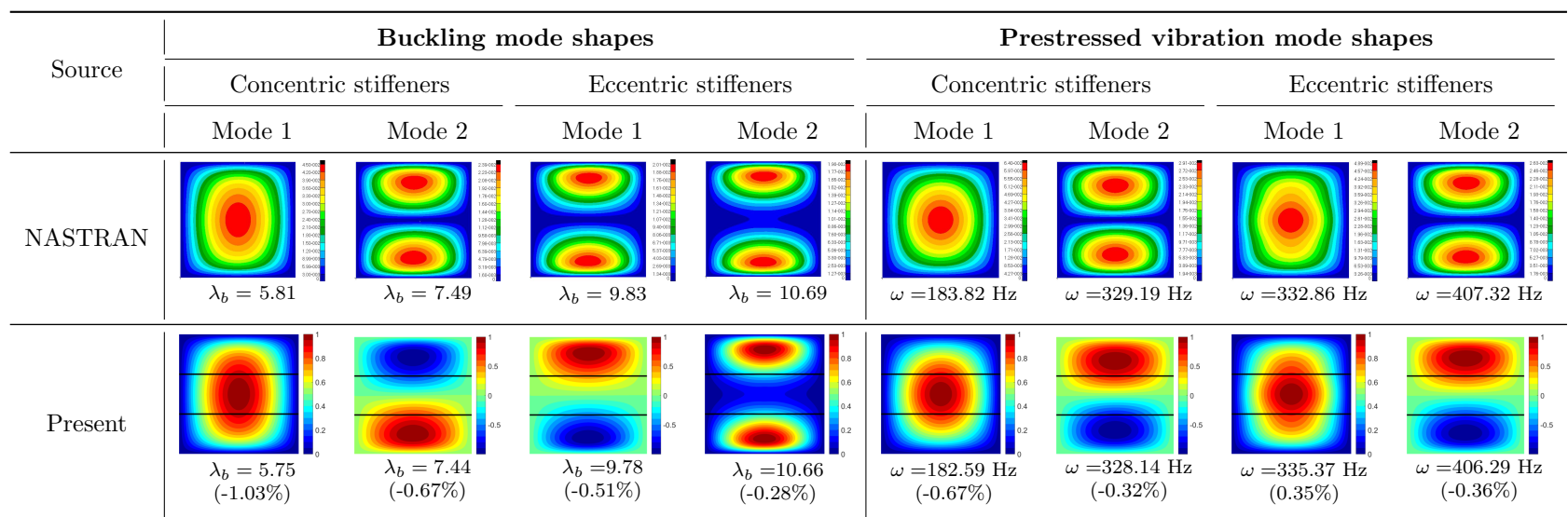


Figure 10: Comparisons of buckling and prestressed vibration mode shapes between NASTRAN and present results for stiffened, VAT laminates with two straight stiffeners

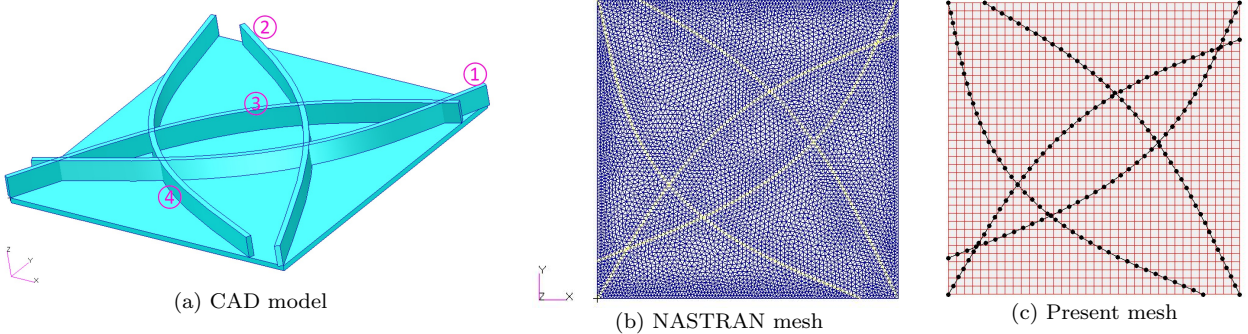


Figure 11: A square panel with NLV fiber path laminates and four arbitrarily shaped stiffeners

Table 4 shows the convergence and verification study results of using present method for prestressed vibration analysis. The mesh for the plate is fixed, 32×32 . There is around 1% change in the first 10 modal frequencies when doubling the stiffener beam elements number from 20 to 40. Hence, it is concluded that the results for the stiffened plate computed with 20 beam elements for each stiffener are converged. The converged results match well with the NASTRAN results. The first two buckling and prestressed vibration mode shapes are examined as seen in Fig. 12. They are in a good agreement with those obtained using NASTRAN. The NASTRAN input files for this case can be found in Appendix C.

Study results show that the present method allows one to conduct the convergence study for the NLV fiber path laminated plate and the stiffeners separately. Unlike a NASTRAN model, for which when there is any small change in the stiffener shape, there will be a change in the whole mesh. In addition to the benefits of the present method as shown in previous works [13, 37] on studying the structural responses of curvilinearly stiffened plates, a fixed converged plate mesh reduces the preprocessing time for evaluating the fiber path angle for each layer of each element for the subsequent the plate's elastic stiffness computation. Especially for the stiffened VAT laminated panels used in the wing skins, the present method saves preprocessing time for local panel optimization studies.

Note that this section is mainly used to demonstrate the capability of using the present method to model the plate and stiffeners separately, especially for the grid stiffened composite plate with bio-inspired shaped stringers [48]. Considering that the primary focus of this work is to develop an accurate structural analysis method to investigate the effect of spatially varying fiber path on stiffened plate's prestressed vibration responses, future work will study the combined effect of using curvilinear stiffeners and the curved fiber path on structural response through an optimization study.

Table 4: Mesh convergence and verification studies of prestressed modal frequencies, ω (unit: Hz), of curvilinearly stiffened NLV fiber path laminated plate with respect to stiffener elements number, for the case of a uniform end-shortening, $\Delta u_0 = 2 \times 10^{-5}$ m

Mode	Concentric stiffeners, $e = 0$						Eccentric stiffeners, $e \neq 0$					
	5	10	20	40	NASTRAN	Diff.	5	10	20	40	NASTRAN	Diff.
1	193.155	198.08	200.68	202.163	204.34	-1.79%	309.77	327.50	338.24	343.42	336.41	0.54%
2	457.025	464.54	469.79	472.458	477.47	-1.61%	677.77	704.76	728.24	740.61	720.39	1.09%
3	498.056	505.16	511.49	514.900	522.25	-2.06%	723.42	754.44	782.45	795.61	769.60	1.67%
4	738.225	746.77	754.53	758.249	768.16	-1.77%	889.47	920.54	944.56	956.78	952.67	-0.85%
5	826.709	843.70	855.90	861.464	875.25	-2.21%	1070.01	1111.28	1137.73	1150.51	1148.54	-0.94%
6	979.405	992.70	1007.97	1015.298	1033.14	-2.44%	1166.11	1199.99	1224.88	1236.34	1245.01	-1.62%
7	1086.942	1097.83	1107.94	1113.045	1126.36	-1.64%	1237.28	1287.22	1330.46	1345.99	1319.14	0.86%
8	1178.073	1199.91	1216.73	1223.402	1244.45	-2.23%	1429.07	1497.48	1542.86	1563.79	1549.75	-0.45%
9	1252.928	1287.54	1310.98	1323.388	1354.80	-3.23%	1467.08	1558.08	1616.69	1641.03	1629.65	-0.79%
10	1457.240	1467.22	1484.58	1492.591	1512.27	-1.83%	1612.18	1647.22	1677.59	1694.96	1684.19	-0.39%

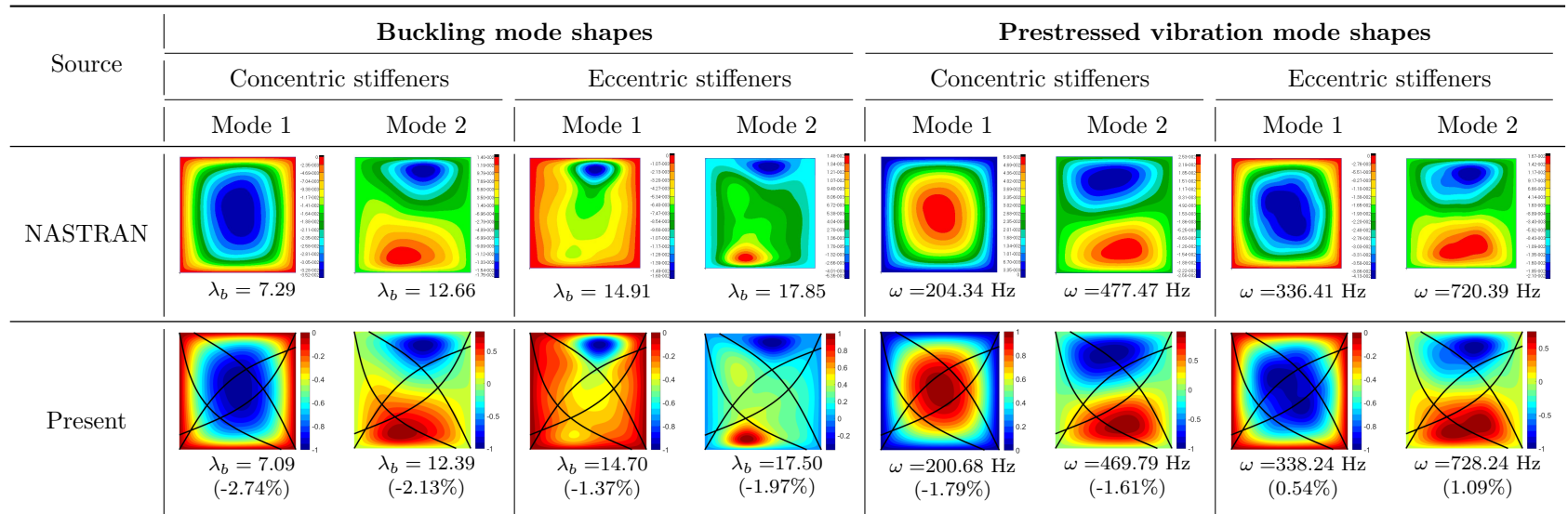


Figure 12: Comparisons of buckling and prestressed vibration mode shapes between NASTRAN and present results for curvilinearly stiffened, VAT laminates

V. Parametric Studies of Fiber Path on Buckling, Free and Prestressed Vibration Responses

From the previous studies, we can conclude that the present program can accurately predict the buckling, free vibration and prestressed vibration responses of a composite plate with both arbitrarily shaped stiffeners and various types of fiber paths. An in-plane uniform end-shortening along the x -axis is used for studying the effect of the fiber path on the prestressed vibration responses. A parametric study is first conducted by employing a linearly varying fiber path along the in-plane end-shortening direction, *i.e.*, x -axis, for the VAT laminated plate. Two parameters, θ_0 at the plate center $x = a/2$, and θ_1 at the plate edges $x = 0$ and $x = a$, are considered and each of them ranges from -90 to 90 degrees. Two straight stiffeners, as studied in Section IV-A, are considered in this parametric study. All geometric dimensions and material properties used in the parametric studies are described in Section IV-A.

In this paper, a stiffened QI laminated plate with common laminate layups of $[\pm 45, 0, 90]_s$ is considered to study the increase in the vibration responses for stiffened plates with both straight fiber path and VAT laminates. Additionally, the buckling end-shortening for the stiffened QI laminates is used as the in-plane compression for studying the prestressed vibration responses of the stiffened, VAT laminates. Eight-layer symmetric laminates $[\pm \langle \theta_0 | \theta_1 \rangle]_{2,s}$ are considered. For convenience, the LV fiber path laminates is denoted as $\langle \theta_0 | \theta_1 \rangle$ in the parametric study.

Based on our previous work [13] and the results by Mittelstedt [49], regardless of stiffeners being concentric or eccentric, the stiffeners are mainly used to change the plate's boundary conditions by modifying the global buckling and vibration mode shape wavelengths for improving the prestressed vibration responses. In this work, we use concentric stiffeners. The mesh size for the plate is fixed at 32×32 and each stiffener is modeled by using 20 beam elements. Two straight equidistant stiffeners along x -axis are considered.

A. Boundary Conditions

Research studies by Honda *et al.* [25] showed that the boundary conditions affect the fundamental frequency of a VAT laminated plate significantly. Hence, in this work, we consider three representative boundary conditions, shown in Fig. 13 for the out-of-plane motion. For the pre-buckling analysis, the boundary condition is same with those as shown in Fig. 9b in Section IV-A.

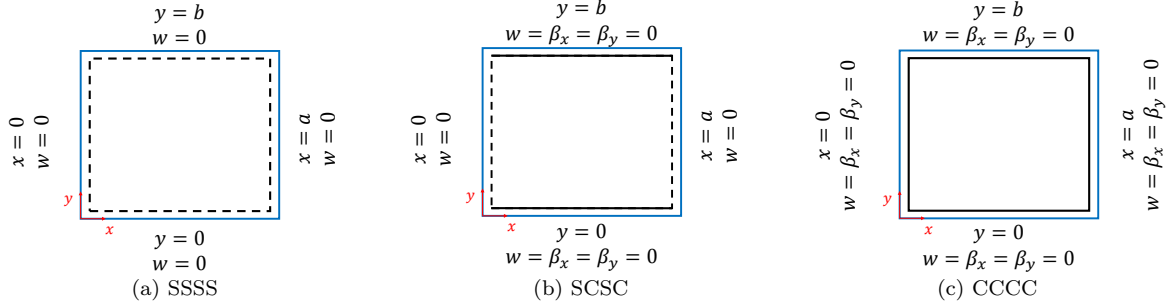


Figure 13: Three different out-of-plane boundary conditions

B. Stiffened QI Laminated Plate

Prestressed vibration analysis of the stiffened QI laminated plates is first conducted. The normalized prestressed vibration eigenvalue, $\bar{\lambda}_v = \lambda_v \frac{a^4 \rho}{E_1 t_p^2}$, is studied at different in-plane end-shortening, Δu , up to the static buckling load and λ_v is the eigenvalue computed from the prestressed vibration analysis. For a linearly prestressed vibration analysis, the normalized prestressed vibration eigenvalue corresponding to the first vibration mode changes linearly with the load factor as expected. The NASTRAN results are also shown here for a further verification. Figure 14 shows that the present results agree well with those obtained from NASTRAN. Static buckling load factor for each boundary condition is shown in the Fig. 14. In this study, $\Delta u = 2 \times 10^{-5}$ m is used. The vibration fundamental frequencies and the buckling loads for the stiffened QI laminated plates with the three different boundary conditions will be used in the subsequent studies for normalization.

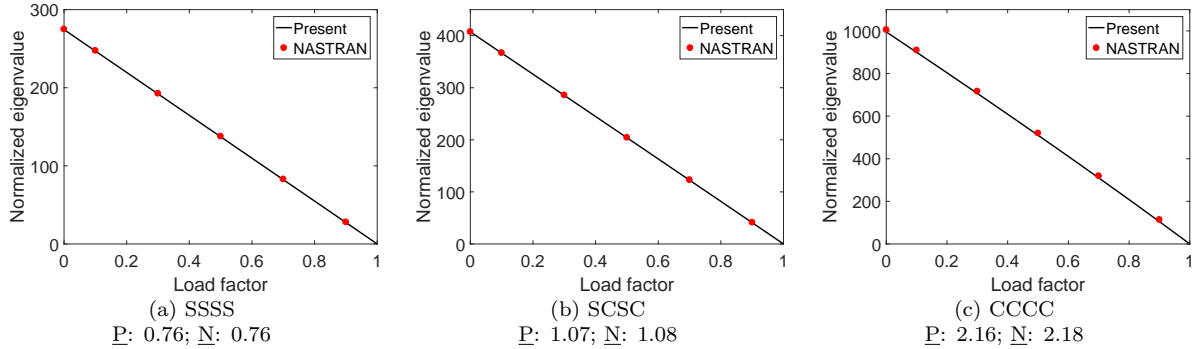


Figure 14: Variation of the first mode normalized prestressed vibration eigenvalue, $\bar{\lambda}_v$, with the applied load up to the static buckling load, \underline{P} : present buckling eigenvalue; \underline{N} : NASTRAN buckling eigenvalue

C. Buckling and Free Vibration Responses

For a plate subjected to an in-plane end-shortening, the prestressed vibration response depends on both the elastic stiffness and the geometric stiffness. Hence, both the free vibration and buckling responses are studied. The critical buckling load for the stiffened plate is computed as [19]:

$$P_{cr} = \lambda_{b,cr} \left[\int_{-b/2}^{b/2} N_{xx}(a,y)dy + \sum_{i=1}^2 A_{s,i}\sigma_{s,i} \right] \quad (13)$$

where $A_{s,i}$ and $\sigma_{s,i}$ is the cross-sectional area and axial stress of the i -th stiffener, respectively. The value of P_{cr} is then used to compute the normalized buckling parameter, $K_{cr} = \frac{P_{cr}a^2}{E_1bt_p^3}$.

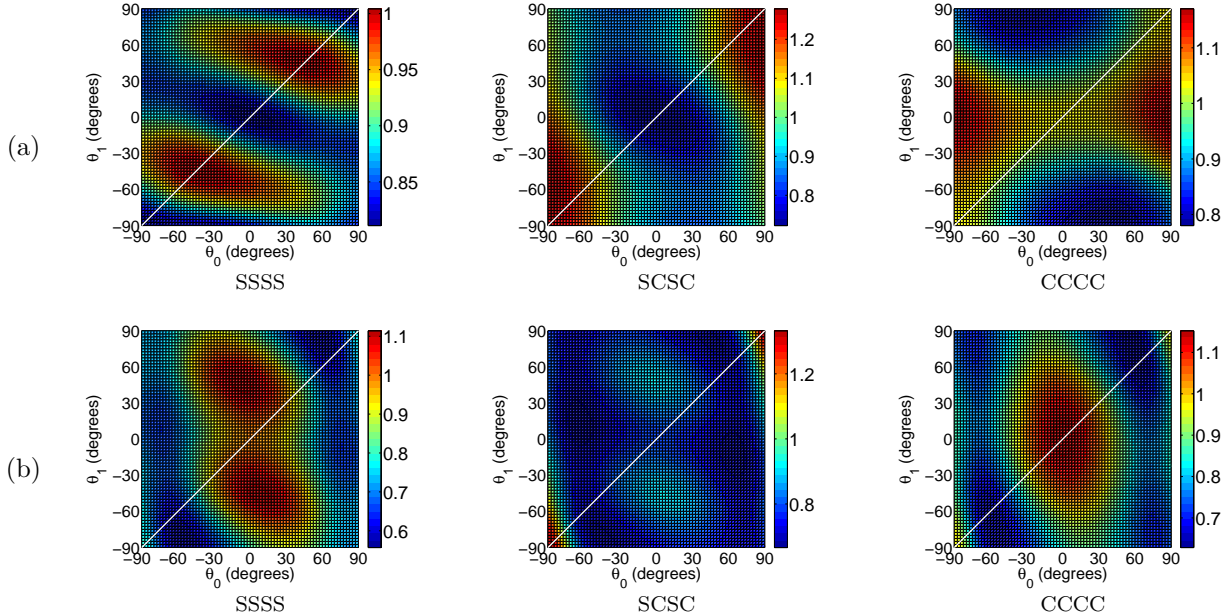


Figure 15: (a) normalized free vibration fundamental frequency $\omega_v/\omega_{v,QI}$ (b) normalized buckling parameter, $K_{cr}/K_{cr,QI}$ for the stiffened plate

Parametric studies on both the free vibration fundamental frequency and the buckling load in terms of the two fiber path angles, θ_0 and θ_1 , are shown in Fig. 15. The diagonal line in white shows the changes in the buckling and vibration responses in terms of the fiber path angle for the straight fiber path laminates. It is observed that the critical buckling load for the laminate layups of $\langle\theta_0|\theta_1\rangle$ equals that with $-\langle\theta_0|\theta_1\rangle$. The changes in the buckling and free vibration responses with the fiber path angles, for the unstiffened plate, are also studied. These are, however, not shown here for brevity. They can be found in the supplemental material in Sections 2.1 and 2.2 of [Supp_Data.pdf](#). It is found that the varying fiber path angles influence the free vibration (Fig. 15(a)) and buckling (Fig. 15(b)) responses differently.

1. Free vibration responses

Table 5 shows the maximum fundamental frequencies and their corresponding fiber paths for both the unstiffened and stiffened laminated plates obtained from parametric studies. Based on the assumption that there is no change in the mass distribution due to the change in the fiber path orientation, the VAT laminates are used to tailor the plate's stiffness distribution to increase the fundamental frequency. It is observed that, for the same boundary conditions, the present LV fiber paths for the maximum fundamental frequency for both the unstiffened and stiffened plates are almost identical. The fiber path angles of $\langle 90^\circ | 90^\circ \rangle$ and $-\langle 90^\circ | 90^\circ \rangle$ are same laminate layups. We only show $\langle 90^\circ | 90^\circ \rangle$ in Table 5.

Table 5: Maximum free vibration fundamental frequency, ω_v (Hz) and the corresponding fiber path for both unstiffened and stiffened laminated plates obtained from parametric studies

Boundary condition	Unstiffened laminated plate			Stiffened laminated plate		
	QI	SF	VAT	QI	SF	VAT
SSSS	71.48	72.65 (1.63%) $\pm\langle 45.0^\circ 45.0^\circ \rangle$	72.65 (1.63%) $\pm\langle 45.0^\circ 45.0^\circ \rangle$	89.68	90.69 (1.12%) $\pm\langle 45.0^\circ 45.0^\circ \rangle$	90.69 (1.12%) $\pm\langle 45.0^\circ 45.0^\circ \rangle$
SCSC	95.32	119.92 (25.80%) $\langle 90^\circ 90^\circ \rangle$	121.83 (27.81%) $\pm\langle 90^\circ 52.5^\circ \rangle$	109.24	130.00 (19.01%) $\langle 90^\circ 90.0^\circ \rangle$	132.32 (21.13%) $\pm\langle 90^\circ 52.5^\circ \rangle$
CCCC	119.06	123.06 (3.35%) $\langle 0^\circ 0^\circ \rangle$ and $\langle 90^\circ 90^\circ \rangle$	140.63 (17.96%) $\pm\langle 90^\circ -2.5^\circ \rangle$	170.78	173.46 (1.57%) $\langle 90.0^\circ 90.0^\circ \rangle$	189.21 (10.79%) $\pm\langle 90.0^\circ 0.0^\circ \rangle$

Note: the percentage values in the bracket are computed with respect to the structure with QI laminates

There is a very slight difference in the VAT laminate configurations for the unstiffened plate ($\pm\langle -90.0^\circ | 2.5^\circ \rangle$) and the stiffened laminated plate ($\pm\langle -90.0^\circ | 0^\circ \rangle$) with the CCCC boundary conditions. The LV fiber path for each layer corresponding to the maximum free vibration fundamental frequency becomes almost perpendicular to the clamped edges. These findings are consistent with those of Honda *et al.* [25] who used B-Spline to parameterize the fiber path for a VAT laminated plate and found that (a) the VAT fiber path has a little effect in improving the free vibration response for a simply-supported plate and (b) the fiber path is oriented to be almost perpendicular to the clamped edges for maximizing the fundamental frequency of the unstiffened laminated plate.

Based on the fact that the out-of-plane motion dominates the first vibration mode shape, the constitutive matrix D_{ij} relates the out-of-plane bending moment and bending curvature, which can be tailored by fiber path orientation using the VAT laminates. The clamped boundary condition affects the bending curvature at the plate's edges and hence influences the fundamental frequency significantly as compared to that with a simply-supported boundary condition where the bending curvature are not restrained.

2. Buckling responses

Table 6 shows the maximum buckling load and their corresponding laminate configurations for both the unstiffened and stiffened laminated plates obtained from the parametric studies. For comparison, the results for the unstiffened plate are also shown in Table 6. When compared to the buckling load for the structure with a QI laminated plate, the improvement in the buckling load of using VAT laminates for the plate is boundary condition dependent.

Table 6: Maximum normalized buckling parameters, K_{cr} , obtained from parametric studies for unstiffened and stiffened laminated plates subjected to a uniform end-shortening

Boundary condition	Unstiffened laminated plate			Stiffened laminated plate		
	QI	SF	VAT	QI	SF	VAT
SSSS	1.22 $\pm\langle 27.5^\circ 27.5^\circ \rangle$	1.15 (-5.74%) $\pm\langle -7.5^\circ 50.0^\circ \rangle$	1.37 (12.30%) $\pm\langle -7.5^\circ 50.0^\circ \rangle$	2.00 $\pm\langle 17.5^\circ 17.5^\circ \rangle$	2.00 (0.00%) $\pm\langle 17.5^\circ 17.5^\circ \rangle$	2.25 (12.50%) $\pm\langle -7.5^\circ 45.0^\circ \rangle$
SCSC	2.07 $\pm\langle 37.5^\circ 37.5^\circ \rangle$	1.57 (-24.15%) $\pm\langle -5.0^\circ 55.0^\circ \rangle$	1.73 (-16.43%) $\pm\langle -5.0^\circ 55.0^\circ \rangle$	2.84 $\pm\langle 90^\circ 90^\circ \rangle$	3.91 (37.68%) $\pm\langle 90^\circ 90^\circ \rangle$	3.91 (37.68%) $\pm\langle 90^\circ 90^\circ \rangle$
CCCC	2.69 $\langle 0^\circ 0^\circ \rangle$	3.62 (34.57%) $\langle 0^\circ 0^\circ \rangle$	3.62 (34.57%) $\langle 0^\circ 0^\circ \rangle$	5.70 $\langle 0.0^\circ 0.0^\circ \rangle$	6.63 (16.23%) $\langle 0.0^\circ 0.0^\circ \rangle$	6.63 (16.23%) $\langle 0.0^\circ 0.0^\circ \rangle$

Note: the percentage values in the bracket are computed with respect to the structure with QI laminates

For the SSSS boundary condition, the VAT laminates shift the maximum stress resultants to the panel's edges for improving the buckling response of both the unstiffened and stiffened laminated plates. The in-plane stress resultants are examined for the stiffened plate and are shown in Fig. 16. It is seen that the maximum values for the stress resultant N_{yy} are shifted to the panel's edges while that is not the case for the dominant axial stress resultant, N_{xx} . The VAT laminates reduce the maximum values of the stress resultants on the peak of the critical mode shape. The in-plane stress resultants and buckling mode results for the stiffened, VAT laminated plate are verified against NASTRAN results and both are in an excellent agreement as seen in Fig. 16.

For the SCSC boundary condition, using both the LV and straight fiber path laminates for the unstiffened plate do not increase the buckling response for the present QI laminated plate. For the stiffened plate, the present LV fiber path laminates for the maximum buckling load obtained from the parametric study are same as the straight fiber path laminates, which are perpendicular to the stiffener direction. For the CCCC boundary condition case, the fiber paths corresponding to the maximum buckling load for both the unstiffened and stiffened plates are same, which lead to a significant increase in the buckling load as compared to that of

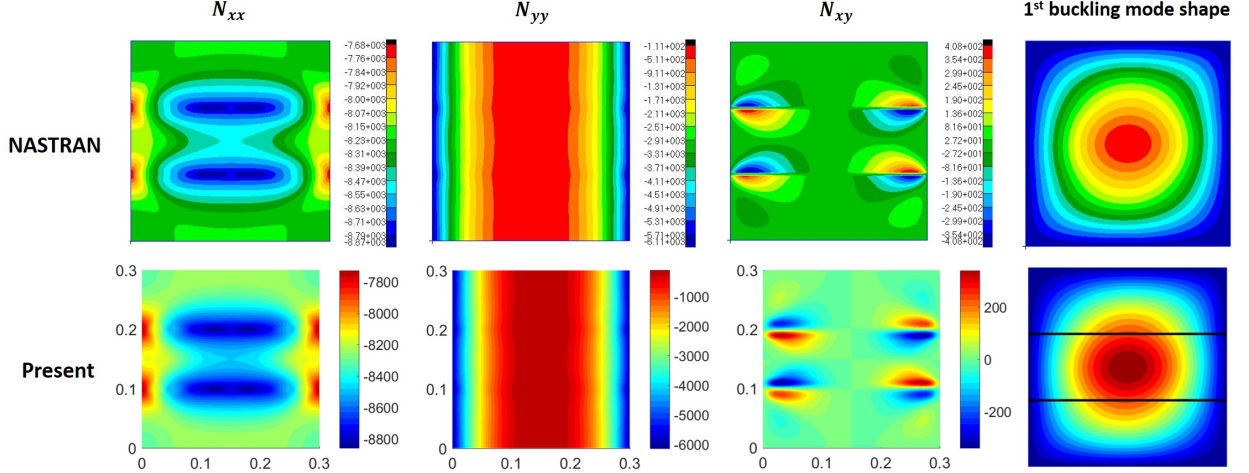


Figure 16: In-plane stress resultants, N_{xx} , N_{yy} and N_{xy} , and critical buckling mode shape for the stiffened plate with SSSS boundary condition, $\Delta u = 2 \times 10^{-5}$ m (Present: $\lambda_b = 0.5448$ and NASTRAN: $\lambda_b = 0.5461$)

using QI laminated plate. For plates with clamped edges, the LV fiber paths tailor the elastic stiffness rather than redistributing the in-plane stress resultants by shifting the maximum stress resultants to panel's edges for improving the buckling responses for stiffened, VAT laminated. Hence, the in-plane stress resultants for these two boundary condition cases are not shown.

Based on the parametric study results in the buckling and free vibration responses, the present LV fiber path appears to be more efficient in improving the buckling response for the stiffened plate with the SSSS boundary condition than in improving the free vibration responses. However, for the stiffened plate with the SCSC and CCCC boundary conditions, the present LV fiber path laminates seem to be more efficient in improving the free vibration response but not in increasing the buckling load. Hence, it is interesting to investigate the effect of the VAT laminates on stiffened plates' prestressed vibration response under various boundary conditions.

D. Prestressed Vibration Responses

To study the effect of VAT laminates on the plate's prestressed vibration responses, parametric studies are conducted for the stiffened, VAT laminates subjected to an in-plane end-shortening at different factors up to the buckling end-shortening for the QI laminated plate. As expected, the normalized eigenvalues for both unstiffened and stiffened QI laminated plates decrease linearly with the in-plane load factor as seen in Fig. 17. When the in-plane load equals the buckling load, the first eigenvalue becomes zero from the linearly prestressed vibration analysis. For comparison, the results for the unstiffened laminates are also shown here.

Note that the buckling loads for the QI laminated structure are different for different boundary conditions.

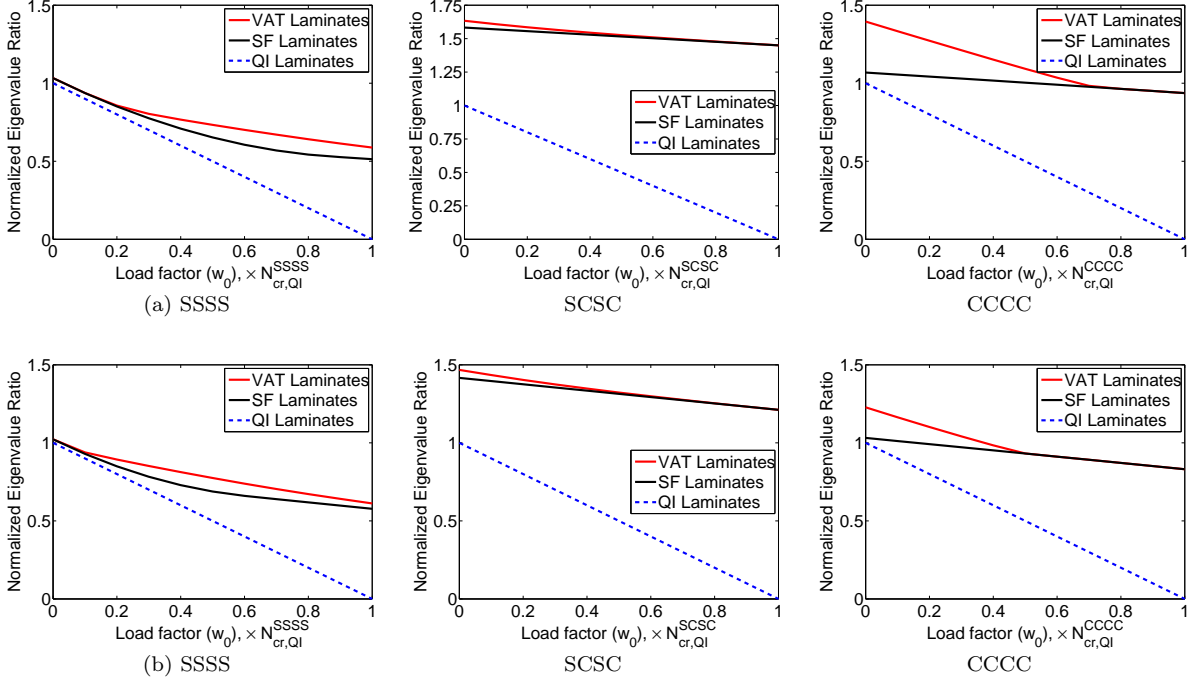


Figure 17: Maximum normalized eigenvalue for the prestressed vibration of (a) unstiffened plate and (b) stiffened plate in terms of the applied in-plane load factor, w_0 , with three different boundary conditions

Figure 17 shows that, for the same boundary condition, the changes in the normalized eigenvalue with the in-plane load factor are almost similar for the unstiffened and stiffened plates. It is observed that the VAT laminates can improve the prestressed vibration responses for both unstiffened and stiffened plates. However, the improvement in the maximum prestressed vibration eigenvalue of using VAT laminates depends on both boundary condition and the in-plane end-shortening.

When the in-plane load factors are small, the LV fiber path laminates increase the prestressed vibration eigenvalues to larger values for both unstiffened and stiffened plates with the SCSC and CCCC boundary conditions. However, there is a little increase in the prestressed vibration eigenvalue for both the simply-supported unstiffened and stiffened plates. When the in-plane load factor becomes large, the LV fiber path laminates become more efficient in improving the prestressed vibration response for both the simply-supported unstiffened and stiffened plates. However, the present LV fiber paths become same with the straight fiber paths for the unstiffened and stiffened plates with both SCSC and CCCC boundary conditions.

It is also observed that the maximum eigenvalue does not change linearly with the in-plane load factor for each boundary condition. The fiber paths obtained from the parametric studies for both LV and straight fiber

paths for the stiffened plate under three representative load factors, 10%, 50% and 100%, are summarized and shown in Fig. 18. The fiber paths for the maximum eigenvalue are different at different in-plane loads, which lead to the change in the maximum normalized eigenvalue that does not vary linearly with the in-plane load factor. The fiber paths corresponding to the maximum eigenvalue for the unstiffened plates are also studied and they are almost same with the those for the stiffened plate. For brevity, the fiber paths for unstiffened plates are not shown but can be found in the supplemental material in Section 2.3 of [Supp_Data.pdf](#).

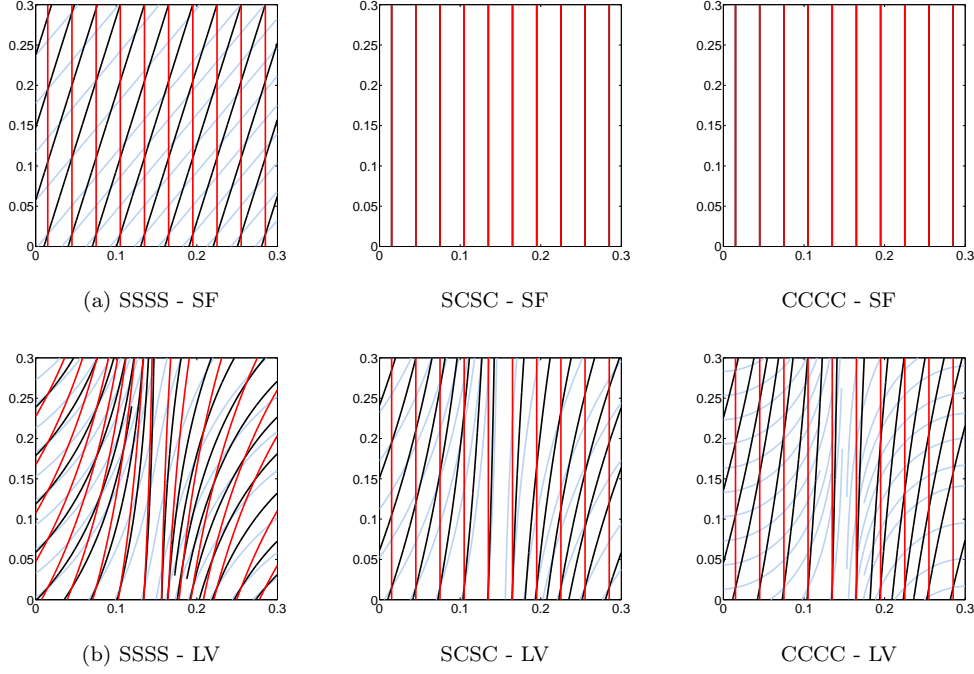


Figure 18: Straight and LV fiber path orientations for **stiffened plates**, $10\% N_{cr,QI}$ (—), $50\% N_{cr,QI}$ (—) and $100\% N_{cr,QI}$ (—), with three different boundary conditions, corresponding to the maximum eigenvalues in parametric studies; the first layer for each case is shown here.

For the SSSS boundary condition case, when the in-plane load factor is very small, the normalized eigenvalues for the straight fiber and VAT laminated plate are very close because the straight fiber laminates have the maximum free vibration fundamental frequency as seen in Table 5. As the in-plane load factor increases, the straight fiber paths gradually become perpendicular to the stiffeners. The LV fiber paths also become almost perpendicular to the stiffeners with the load factor but still remains curved, resulting in a large value in the prestressed vibration fundamental frequency.

For the SCSC boundary condition case, it seems that the LV fiber paths have the same effect with the straight fiber paths in improving the stiffened plate's buckling response. Because the optimal straight fiber path laminates for the maximum buckling load and the free vibration fundamental frequency are same,

$\langle 90|90 \rangle$, the optimal straight fiber paths corresponding to the maximum prestressed vibration eigenvalue are same for all load factors. A linear change in the maximum normalized eigenvalue with the load factor is observed as expected. The straight fiber path of $\langle 90|90 \rangle$ is found to have a slightly lower value in free vibration modal frequency than the present LV fiber path laminates but it has the maximum buckling load in the parametric study. The LV fiber paths become straight and perpendicular to the clamped edges with the load factor for improving the prestressed vibration fundamental frequency.

For the CCCC boundary condition case, the optimal straight fiber path for the maximum normalized eigenvalue becomes perpendicular to the stiffeners and remains same with the in-plane load factor. For the lower in-plane load factors, VAT laminates are much more efficient in improving the prestressed vibration response. This is because the VAT laminates allow their fibers being almost perpendicular to the clamped edges to improve the free vibration response. As the in-plane load factors increases, the LV fiber paths become same with the straight fiber paths, both being perpendicular to the stiffeners for improving the stiffened plate's prestressed vibration response.

Parametric studies show that the fiber path corresponding to the maximum free vibration fundamental frequency gradually changes with the in-plane load factor for improving the prestressed vibration responses. The fiber path at the larger in-plane load factor corresponding to the maximum prestressed vibration frequency is not same as the one for the maximum buckling load. Except for the case for the stiffened plate with the SCSC boundary condition, this is because the fiber paths for the maximum buckling load and the maximum free vibration fundamental frequency are same. To study how the fiber path influences the prestressed vibration response through tailoring the elastic stiffness or the effective (elastic plus geometric) stiffness, we use optimization for studying the effect of an NLV fiber path in improving the plate's prestressed vibration response.

VI. Nonlinear Varying Fiber Path for Buckling, Free and Prestressed Vibration Responses

As a further investigation into using VAT laminates for improving a laminated plate's prestressed vibration responses, this section considers laminates with NLV fiber paths whose fiber path angles are parameterized using Lagrange polynomials, $NLV(x, y)$, as given in Section II-D. To reduce the computational effort, we consider $\Theta_1 = \Theta_2$ as seen in Fig. 2 in this section. For the case of three uniform reference points along both the x - and y -axes, there are 9 design variables for the fiber path angles at 9 reference points. Pre-

viously developed parallel particle swarm optimization code [50] is used as the optimizer. The optimization parameters and convergence criteria can be found in previous work [50], which will not be shown here for brevity. Optimization studies using NLV fiber paths for the stiffened plate with different boundary conditions are conducted.

A. Free Vibration and Buckling Responses

Optimization results for the maximum free vibration fundamental frequency and the buckling load are shown in Table 7 for the stiffened plate with different boundary conditions. For all cases, the NLV fiber paths are found to have a slight improvement, less than 2.5% for the stiffened plate's free vibration fundamental frequency. However, the NLV fiber path laminates have a significant improvement in the buckling load, up to 44.04%, for the stiffened plate as compared to that using the LV fiber path laminates.

Table 7: Maximum free vibration frequency, ω_v (Hz) and buckling load parameter for the stiffened plate using NLV fiber path laminates obtained from optimization studies

Boundary condition	Free vibration fundamental frequency, ω_v			Critical buckling load parameter, K_{cr}		
	LV	NLV	improvement	LV	NLV	improvement
SSSS	90.69	90.71	0.02%	2.25	2.88	28.00%
SCSC	132.32	135.36	2.30%	3.91	4.68	19.69%
CCCC	189.21	193.50	2.27%	6.63	9.55	44.04%

The optimal NLV fiber paths corresponding to the maximum free vibration frequency for each boundary condition are shown in Fig. 19. For comparison, the straight and LV fiber paths corresponding to the maximum free vibration fundamental frequency obtained from the parametric study in Section V are also included. It is observed that the optimal NLV fiber paths, which are very close to the LV fiber paths, lead to a slight increase in the free vibration fundamental frequency. The free vibration mode results for the stiffened plate with the optimal NLV fiber paths have been verified with a good agreement with the NASTRAN results. The free vibration mode results comparison and the optimal NLV fiber paths are given in the supplemental material in Section 3 of [Supp_Data.pdf](#). Based on the assumption that the mass distribution does not change with the fiber path angles, it can be concluded that the NLV fiber path has little effect in tailoring the stiffened plate's elastic stiffness towards increasing its free vibration fundamental frequency.

The optimal NLV fiber paths for the maximum buckling load for each boundary condition case are also compared against the straight and LV fiber paths as shown in Fig. 20. It is seen that the optimal NLV fiber

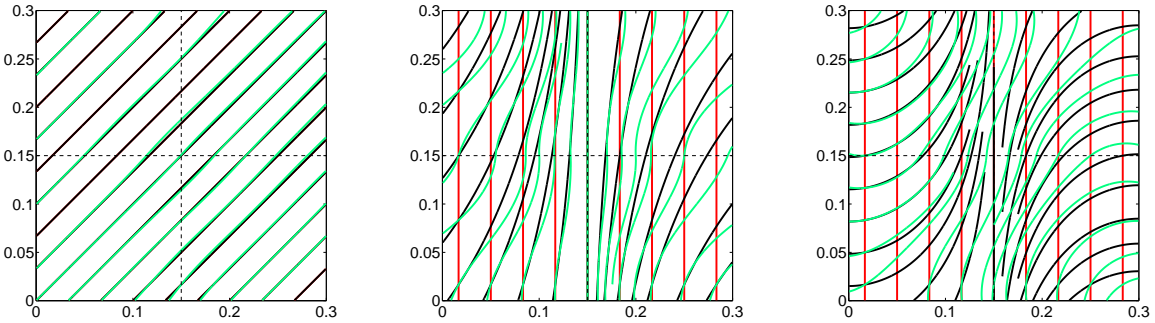


Figure 19: Optimal fiber paths for the maximum free vibration fundamental frequency of stiffened plate with three different boundary conditions, SF (—), LV (—) and NLV (—); first layer fiber path is shown here

paths are significantly different from both the straight and LV fiber paths. Also, the optimal NLV fiber paths for the maximum buckling load for each boundary condition are different from the ones for the maximum free vibration fundamental frequency, as shown in Fig. 19.

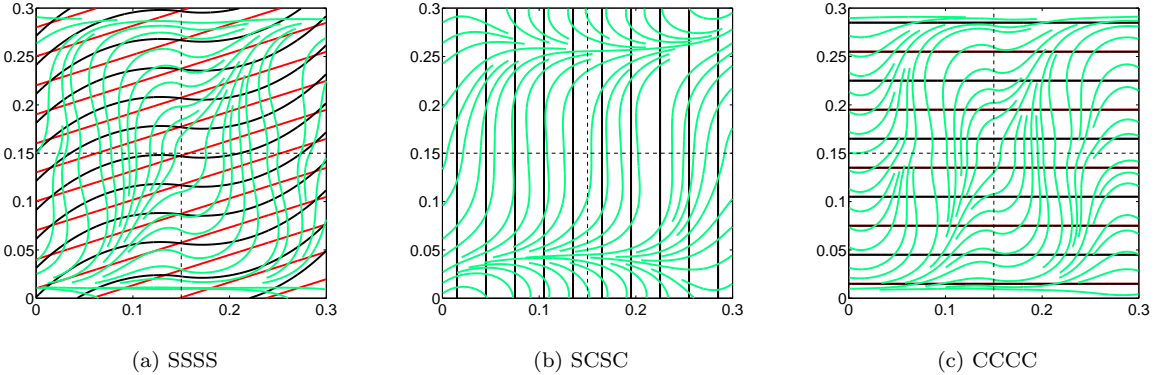


Figure 20: Optimal fiber paths for the maximum buckling load of stiffened plates with three different boundary conditions, SF (—), LV (—) and NLV (—); first layer fiber path is shown

The in-plane stress resultants for each boundary condition case are computed and shown in Fig. 21. It is clearly seen that the dominant stress resultant with the maximum magnitudes, N_{xx} , are shifted to the panel's edges while this is not observed in the LV fiber path laminate case as seen in Fig. 16. Additionally, the maximum stress resultants, N_{yy} and N_{xy} , at the plate's center are also reduced for improving the plate's buckling responses. It can be concluded that one can use the NLV fiber paths to further improve the structural total buckling response by modifying the in-plane stress resultants distribution into a favorable one as compared to that using LV fiber paths. Note that the in-plane stress resultants and buckling mode results for the stiffened plate with NLV fiber path laminates have been compared against NASTRAN results.

For brevity, they are not shown here but the results comparison and the optimal NLV fiber paths can be found in the supplemental material in Section 4 of [Supp_Data.pdf](#).

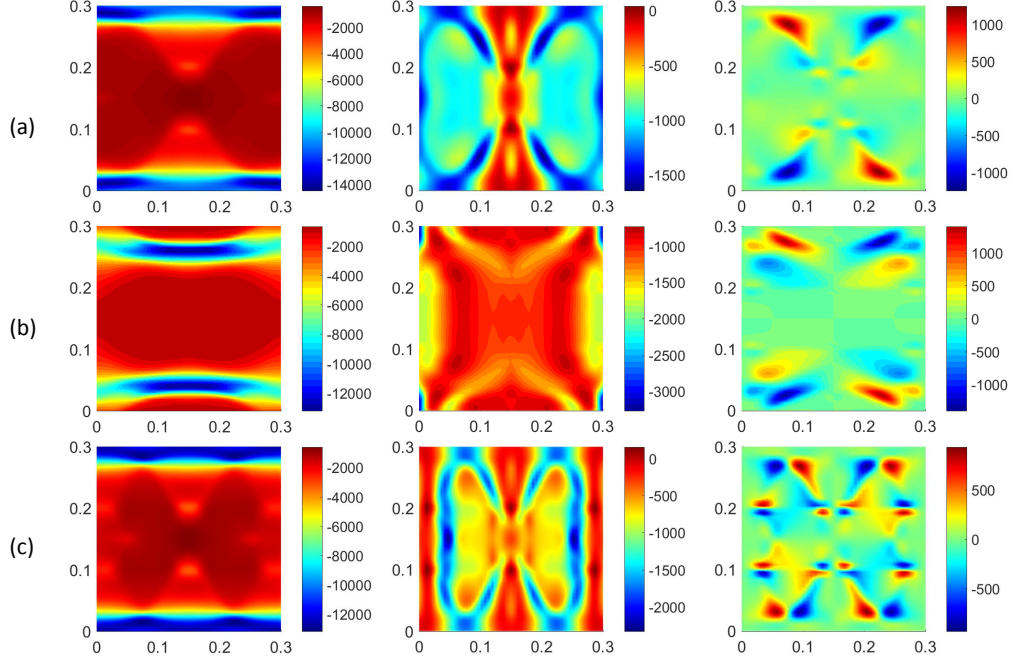


Figure 21: In-plane stress resultants, N_{xx} , N_{yy} and N_{xy} , for the stiffened plate with three boundary condition cases, $\Delta u = 2 \times 10^{-5}$ m

Although no study is available on using LV fiber path along the y -axis, based on the optimal fiber path in Figs. 19 and 20 and the number of design variables used in the present NLV fiber paths, one still can conclude that the NLV fiber path can further increase the buckling load but only leads to a slight increase in the free vibration fundamental frequency.

B. Prestress Vibration Responses

Optimization studies for maximizing the prestressed vibration fundamental frequency of the stiffened plate at three representative load factors are also conducted. Optimization results, summarized in Table 8, show that the NLV fiber paths can further increase the prestressed normal vibration frequency for the stiffened plate under various in-plane loads. However, the improvement is much less than that for the buckling eigenvalue but is slightly larger than that for the free vibration fundamental frequency.

For each boundary condition case, the optimal fiber paths corresponding to the maximum prestressed vibration fundamental frequency at the three representative in-plane loads are shown in Fig. 22. It can be seen that the optimal fiber paths are very similar at the three load cases, for each boundary condition

Table 8: Maximum prestressed vibration fundamental frequency (Hz) of the stiffened plates under different in-plane end-shortenings

Boundary conditions	10% $N_{cr,QI}$			50% $N_{cr,QI}$			100% $N_{cr,QI}$		
	LV	NLV	improvement	LV	NLV	improvement	LV	NLV	improvement
SSSS	86.90	87.99	1.25%	78.93	80.62	2.14%	70.15	73.10	4.21%
SCSC	130.83	133.79	2.26%	125.62	128.58	2.36%	120.24	122.66	2.01%
CCCC	184.25	189.17	2.67%	164.90	176.21	6.86%	155.67	161.94	4.03%

case. The optimal fiber paths become almost perpendicular to the stiffeners at the plate's center but not purely straight as the one shown in Fig. 18. The optimal fiber paths for the plate with the CCCC boundary condition are also almost perpendicular to the four clamped edges. The optimal NLV fiber paths for all cases can be found in the supplemental material in Section 5 of [Supp_Data.pdf](#). The prestressed vibration results in this section are not verified using NASTRAN as they have been verified extensively in Section IV.

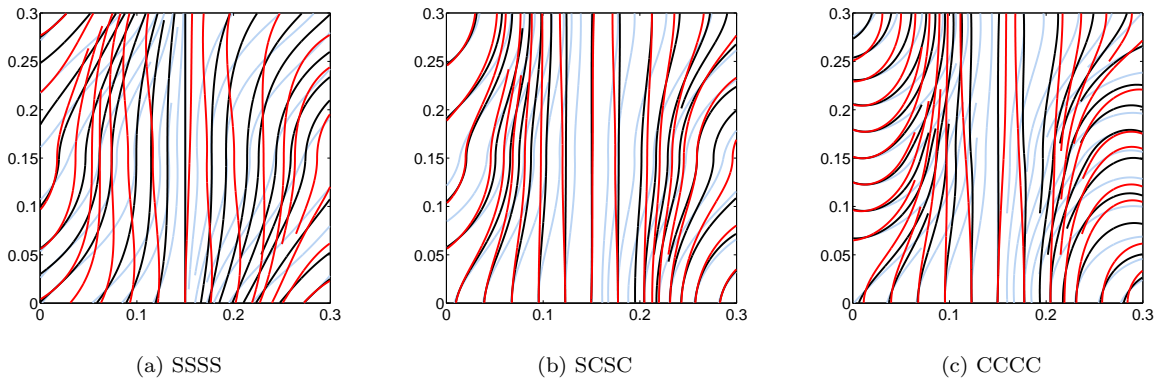


Figure 22: Optimal NLV fiber path orientations, $10\% N_{cr,QI}$ (light blue), $50\% N_{cr,QI}$ (black) and $100\% N_{cr,QI}$ (red), with three different boundary conditions; the first layer for each case is shown

For the simply-supported stiffened plate, even though there is almost no increase (0.02%) in the plate's free vibration response when using NLV fiber paths, it is still possible to use NLV fiber paths to tailor the effective stiffness for improving its prestressed vibration response. This is because a significant improvement in the buckling load (28%) can be obtained when using NLV fiber path laminates. For the SCSC boundary condition case, the optimal fiber path becomes almost perpendicular to the clamped edges and stiffeners for improving the prestressed vibration response. For the CCCC boundary condition case, the optimal NLV fiber paths become almost perpendicular to all clamped edges. The optimal fiber paths for the two boundary cases are similar to those for the maximum free vibration frequency. This means that for the stiffened plate with

the SCSC and CCCC boundary conditions, the optimal NLV fiber paths appear to increase the structural elastic stiffness for improving the prestressed vibration responses at different in-plane loads.

VII. Conclusion

This paper studies the prestressed vibration responses of a stiffened, VAT laminated plate subjected to a uniform in-plane end-shortening for plates with different boundary conditions. Considering the spatial dependence of both the stiffeners and the fiber path angles, we model the VAT laminated plate and the stiffeners separately in the finite element model. This method obviates the requirement to place both the plate and the stiffeners' finite element nodes along the stiffener-plate and the stiffener-stiffener interfaces, as is the case for a traditional finite element model. The displacement compatibility at the interfaces is enforced using a transformation matrix. This method allows one to study the mesh convergence for the plate and the stiffeners, separately, which improves both the efficiency and the robustness of the finite element model. Detailed verification studies on buckling, free and prestressed vibration responses for both the unstiffened and stiffened, VAT laminated plates are conducted. All verification results computed using the present method are in an excellent agreement with the available results in literature and NASTRAN results.

Parametric studies show that the improvements in buckling and free vibration responses, using the present linearly-varying (LV) fiber path for a stiffened plate, depend on the boundary conditions. As compared to the straight fiber path, the present LV fiber path appears to be more effective in improving the buckling response for the simply-supported stiffened plate than in improving the free vibration responses. However, for the stiffened plates with the SCSC and CCCC boundary conditions, the present LV fiber paths seem to be more effective in improving the free vibration response but not towards increasing the buckling loads. The improvements for the prestressed vibration response depend on both the boundary conditions and the applied in-plane end-shortening. When the in-plane end-shortening is small, the present LV fiber paths are more effective for the stiffened plates with SCSC and CCCC boundary conditions. When the in-plane end-shortening becomes larger, the present LV fiber paths become more effective for the simply-supported stiffened plate.

Nonlinearly varying (NLV) fiber path laminates can further increase the buckling loads of stiffened plates for all cases of boundary conditions studied here when compared to those for laminates with the LV fiber paths. The fiber path can tailor all the in-plane stress resultants distribution into a favorable one to improve the buckling response significantly. However, there is almost no increase in the free vibration fundamental frequency of a simply-supported stiffened laminated plate when using the NLV fiber paths. Also, slight

increases in the free vibration fundamental frequency are observed for the stiffened plates with the SCSC and CCCC boundary conditions. Optimization studies also show slight increases in the prestressed vibration fundamental frequency for all the studied cases when using the NLV fiber paths. The effective stiffness can be tailored by using the NLV fiber paths for the simply-supported stiffened plate resulting in an increased prestressed vibration fundamental frequency. For the stiffened plates with the SCSC and CCCC boundary conditions, their optimal NLV fiber paths appear to be similar to those for the maximum free vibration fundamental frequencies, both being almost perpendicular to the clamped edges. It is believed that using more design variables for the NLV fiber paths can further increase the buckling load but may only slightly increase the free vibration fundamental frequency for the stiffened plates with or without the presence of prestress as compared to that of the stiffened laminated plate with the LV fiber paths.

Appendix

A. The fiber path angles, T_{mn} , at reference points in Section II-D are:

$$\Theta_1 : T_{mn} = \begin{bmatrix} 71 & 49.5 & 71.5 \\ 67 & 50 & 51 \\ 17 & 12 & 45 \end{bmatrix} \text{ degrees} \quad \Theta_2 : T_{mn} = \begin{bmatrix} -72.5 & -59 & -59.5 \\ -65 & -54 & -50.5 \\ 14 & 11.5 & 6 \end{bmatrix} \text{ degrees}$$

B. Physical coordinates for four curvilinear stiffeners

Nine representative physical point coordinates for the four curvilinear stiffeners given in Section IV-B are:

- ① : $x = [0.0000, 0.0484, 0.0962, 0.1427, 0.1859, 0.2238, 0.2543, 0.2783, 0.3000];$
 $y = [0.0375, 0.0567, 0.0767, 0.1002, 0.1290, 0.1647, 0.2067, 0.2528, 0.3000];$
- ② : $x = [0.0375, 0.0815, 0.1243, 0.1642, 0.1993, 0.2292, 0.2550, 0.2779, 0.3000];$
 $y = [0.3000, 0.2739, 0.2463, 0.2144, 0.1772, 0.1358, 0.0916, 0.0460, 0.0000];$
- ③ : $x = [0.3000, 0.2521, 0.2049, 0.1601, 0.1193, 0.0840, 0.0534, 0.0262, 0.0000];$
 $y = [0.2625, 0.2438, 0.2235, 0.1983, 0.1667, 0.1294, 0.0878, 0.0442, 0.0000];$
- ④ : $x = [0.2625, 0.2135, 0.1651, 0.1192, 0.0787, 0.0469, 0.0253, 0.0114, 0.0000];$
 $y = [0.0000, 0.0209, 0.0433, 0.0705, 0.1051, 0.1478, 0.1965, 0.2480, 0.3000];$

C. NASTRAN input files

NASTRAN input files for buckling and prestressed vibration analysis of the stiffened, VAT laminated plates with NLV fiber paths under a uniform in-plane end-shortening for verification cases in Section IV are available

in https://github.com/zhaowei0566/SPAD/tree/master/AIAAJ_Paper_Data/prestressed_vibration_VAT_SP

References

- [1] Lazan, B. J., "Fatigue Failure under Resonant Vibration Conditions," 1954, Wright Air Development Center (WADC) Technical Report 54-20, University of Minnesota.
- [2] Grandhi, R. and Venkayya, V., "Structural Optimization with Frequency Constraints," *AIAA Journal*, Vol. 26, No. 7, 1988, pp. 858–866.
- [3] Haftka, R. T. and Gürdal, Z., *Elements of Structural Optimization*, Vol. 11, Springer Science & Business Media, 2012.
- [4] Saravanos, D. and Chamis, C., "An Integrated Methodology for Optimizing the Passive Damping of Composite Structures," *Polymer Composites*, Vol. 11, No. 6, 1990, pp. 328–336.
- [5] Forster, E., Clay, S., Holzwarth, R., Pratt, D., and Paul, D., "Flight Vehicle Composite Structures," *26th Congress of International Council of the Aeronautical Sciences (ICAS)*, Anchorage, Alaska, 2008, AIAA 2008-8976.
- [6] Renton, W. J., Olcott, D., Roeseler, W., Batzer, R., Baron, W., and Velicki, A., "Future of Flight Vehicle Structures (2002 to 2023)," *Journal of Aircraft*, Vol. 41, No. 5, 2004, pp. 986–998.
- [7] Timoshenko, S. P. and Gere, J. M., "Theory of Elastic Stability," The McGraw-Hill Book Company, 1963, pp. 225–228.
- [8] Saravanos, D. A. and Chamis, C., "Multiobjective Shape and Material Optimization of Composite Structures including Damping," *AIAA Journal*, Vol. 30, No. 3, 1992, pp. 805–813.
- [9] Zhao, W. and Kapuria, R. K., "Buckling Analysis of Unitized Curvilinearly Stiffened Composite Panels," *Composite Structures*, Vol. 135, 2016, pp. 365–382.
- [10] Gürdal, Z., Tatting, B. F., and Wu, K. C., "Two-Placement Technology and Fabrication Issues for Laminated Composite Structures," *Proceedings of the 46th AIAA/ASME/ASCE/AHS/ASC Structures, Structural Dynamics and Materials Conference*, Austin, Texas, 2005, AIAA 2005-2017.

- [11] Gürdal, Z. and Olmedo, R., “In-plane Response of Laminates with Spatially Varying Fiber Orientations: Variable Stiffness Concept,” *AIAA Journal*, Vol. 31, No. 4, 1993, pp. 751–758.
- [12] Abdalla, M. M., Setoodeh, S., and Gürdal, Z., “Design of Variable Stiffness Composite Panels for Maximum Fundamental Frequency using Lamination Parameters,” *Composite Structures*, Vol. 81, No. 2, 2007, pp. 283–291.
- [13] Zhao, W. and Kapania, R. K., “Vibration Analysis of Curvilinearly Stiffened Composite Panels Subjected to In-plane loads,” *AIAA Journal*, Vol. 55, No. 3, 2017, pp. 981–997.
- [14] Hyer, M. W. and Charette, R. F., “Use of Curvilinear Fiber Format in Composite Structure Design,” *AIAA Journal*, Vol. 29, No. 6, 1991, pp. 1011–1015.
- [15] Wu, K. C. and Gürdal, Z., “Thermal Testing of Tow-Placed, Variable Stiffness Panels,” *Proceedings of the 42nd AIAA/ASME/ASCE/AHS/ASC Structures, Structural Dynamics and Materials Conference and Exhibit*, Seattle, Washington, 2001, AIAA 2001-1190.
- [16] Wu, K. C., Gürdal, Z., and Starnes, J. H., “Structural Response of Compression-loaded, Tow-placed, Variable Stiffness Panels,” *Proceedings of the AIAA/ASME/ASCE/AHS/ASC 43rd Structures, Structural Dynamics and Materials Conference, Denver, CO*, 2002, AIAA 2002-1512.
- [17] Lopes, C. S., Camanho, P. P., Gürdal, Z., and Tatting, B. F., “Progressive Failure Analysis of Tow-Placed, Variable-Stiffness Composite Panels,” *International Journal of Solids and Structures*, Vol. 44, No. 25, 2007, pp. 8493–8516.
- [18] Lopes, C., Gürdal, Z., and Camanho, P., “Variable-Stiffness Composite Panels: Buckling and First-ply Failure Improvements over Straight-fibre Laminates,” *Computers and Structures*, Vol. 86, No. 9, 2008, pp. 897–907.
- [19] Coburn, B. H., Wu, Z., and Weaver, P. M., “Buckling Analysis of Stiffened Variable Angle Tow Panels,” *Composite Structures*, Vol. 111, 2014, pp. 259–270.
- [20] Wu, Z., Weaver, P. M., Raju, G., and Kim, B. C., “Buckling Analysis and Optimisation of Variable Angle Tow Composite Plates,” *Thin-walled Structures*, Vol. 60, 2012, pp. 163–172.
- [21] Raju, G., Wu, Z., and Weaver, P. M., “Postbuckling Analysis of Variable Angle Tow Plates using Differential Quadrature Method,” *Composite Structures*, Vol. 106, 2013, pp. 74–84.

- [22] Oliveri, V. and Milazzo, A., “A Rayleigh-Ritz Approach for Postbuckling Analysis of Variable Angle Tow Composite Stiffened Panels,” *Computers & Structures*, Vol. 196, 2018, pp. 263–276.
- [23] Ribeiro, P., Akhavan, H., Teter, A., and Warmiński, J., “A Review on the Mechanical Behaviour of Curvilinear Fibre Composite Laminated Panels,” *Journal of Composite Materials*, Vol. 48, No. 22, 2014, pp. 2761–2777.
- [24] Blom, A. W., Setoodeh, S., Hol, J. M., and Gürdal, Z., “Design of Variable-Stiffness Conical Shells for Maximum Fundamental Eigenfrequency,” *Computers and Structures*, Vol. 86, No. 9, 2008, pp. 870–878.
- [25] Honda, S., Narita, Y., and Sasaki, K., “Maximizing the Fundamental Frequency of Laminated Composite Plates with Optimally Shaped Curvilinear Fibers,” *Journal of System Design and Dynamics*, Vol. 3, No. 6, 2009, pp. 867–876.
- [26] Honda, S. and Narita, Y., “Natural Frequencies and Vibration Modes of Laminated Composite Plates Reinforced with Arbitrary Curvilinear Fiber Shape Paths,” *Journal of Sound and Vibration*, Vol. 331, No. 1, 2012, pp. 180–191.
- [27] Akhavan, H. and Ribeiro, P., “Natural Modes of Vibration of Variable Stiffness Composite Laminates with Curvilinear Fibers,” *Composite Structures*, Vol. 93, No. 11, 2011, pp. 3040–3047.
- [28] Rodrigues, J. D., Ribeiro, P., and Akhavan, H., “Experimental and Finite Element Modal Analysis of Variable Stiffness Composite Laminated Plates,” *11th International Conference on Vibration Problems (ICOVP-2013)*, Lisbon, Portugal, 2013.
- [29] Akhavan, H., *Nonlinear Vibration of Tow Placed Variable Stiffness Composite Laminates*, Ph.D. thesis, Universidade Do Porto, Porto, Portugal, 2015.
- [30] Ribeiro, P. and Akhavan, H., “Non-linear Vibrations of Variable Stiffness Composite Laminated Plates,” *Composite Structures*, Vol. 94, No. 8, 2012, pp. 2424–2432.
- [31] Ribeiro, P., “Non-linear Free Periodic Vibrations of Variable Stiffness Composite Laminated Plates,” *Nonlinear Dynamics*, Vol. 70, No. 2, 2012, pp. 1535–1548.
- [32] Stodieck, O., Cooper, J. E., Weaver, P. M., and Kealy, P., “Improved Aeroelastic Tailoring using Tow-Steered Composites,” *Composite Structures*, Vol. 106, 2013, pp. 703–715.

- [33] Stanford, B. K., Jutte, C. V., and Wu, K. C., “Aeroelastic Benefits of Tow Steering for Composite Plates,” *Composite Structures*, Vol. 118, 2014, pp. 416–422.
- [34] Guimaraes, T. A., Castro, S. G., Rade, D. A., and Cesnik, C. E., “Panel Flutter Analysis and Optimization of Composite Tow Steered Plates,” *58th AIAA/ASCE/AHS/ASC Structures, Structural Dynamics, and Materials Conference*, 2017, AIAA 2017-1118.
- [35] Akhavan, H. and Ribeiro, P., “Aeroelasticity of Composite Plates with Curvilinear Fibres in Supersonic Flow,” *Composite Structures*, Vol. 194, 2018, pp. 335–344.
- [36] Hao, P., Yuan, X., Liu, C., Wang, B., Liu, H., Li, G., and Niu, F., “An Integrated Framework of Exact Modeling, Isogeometric Analysis and Optimization for Variable-stiffness Composite Panels,” *Computer Methods in Applied Mechanics and Engineering*, Vol. 339, 2018, pp. 205–238.
- [37] Zhao, W., Singh, K., and Kapania, R. K., “Thermal Buckling Analysis and Optimization of Variable Angle Tow Laminates with Curvilinear Stiffeners,” *AIAA Journal of Spacecraft and Rockets*, 2018, Accepted.
- [38] Langley, P. T., *Finite Element Modeling of Tow-Placed Variable-Stiffness Composite Laminates*, Virginia Polytechnic Institute and State University, 1999.
- [39] Gürdal, Z., Tatting, B. F., and Wu, K., “Variable Stiffness Composite Panels: Effects of Stiffness Variation on the In-Plane and Buckling Response,” *Composites Part A: Applied Science and Manufacturing*, Vol. 39, No. 5, 2008, pp. 911–922.
- [40] Stodieck, O., Cooper, J., Weaver, P., and Kealy, P., “Aeroelastic Tailoring of a Representative Wing Box Using Tow-Steered Composites,” *AIAA Journal*, Vol. 55, No. 4, 2017, pp. 1425–1439.
- [41] Tsai, S. W. and Pagano, N. J., “Invariant Properties of Composite Materials,” *Composite Material Workshop*, Technomic, Westport, PA, 1968, pp. 233–252.
- [42] IJsselmuiden, S. T., Abdalla, M. M., and Gürdal, Z., “Optimization of Variable Stiffness Panels for Maximum Buckling Loads using Lamination Parameters,” *AIAA Journal*, Vol. 48, No. 1, 2010, pp. 134–143.
- [43] Setoodeh, S., Blom, A., Abdalla, M., and Gürdal, Z., “Generating Curvilinear Fiber Paths from Lamination Parameters Distribution,” *47th AIAA/ASME/ASCE/AHS/ASC Structures, Structural Dynamics, and Materials Conference*, 2015, AIAA 2015-1118.

ics, and Materials Conference 14th AIAA/ASME/AHS Adaptive Structures Conference 7th, Newport, Rhode Island, 2006, AIAA 2006-1875.

- [44] Samukham, S., Raju, G., and Vyasarayani, C., “Parametric Instabilities of Variable Angle Tow Composite Laminate under Axial Compression,” *Composite Structures*, Vol. 166, 2017, pp. 229–238.
- [45] Rohatgi, A., “WebPlotDigitizer,” 2011, <https://automeris.io/WebPlotDigitizer/index.html>.
- [46] Zhao, W., Jrad, M., Gupta, R., and Kapania, R. K., “Multidisciplinary Design, Analysis and Optimization of Performance Adaptive Aeroelastic Wings,” *AIAA Atmospheric Flight Mechanics Conference, AIAA SciTech Forum*, Grapevine, Texas, 2017, AIAA 2017-1392.
- [47] Mulani, S. B., Slemp, W. C., and Kapania, R. K., “EBF3PanelOpt: An Optimization Framework for Curvilinear Blade-stiffened Panels,” *Thin-Walled Structures*, Vol. 63, 2013, pp. 13–26.
- [48] Wang, D., Abdalla, M. M., Wang, Z.-P., and Su, Z., “Streamline Stiffener Path Optimization (SSPO) for Embedded Stiffener Layout Design of Non-uniform Curved Grid-stiffened Composite (NCGC) Structures,” *Computer Methods in Applied Mechanics and Engineering*, 2018, DOI: <https://doi.org/10.1016/j.cma.2018.09.013>.
- [49] Mittelstedt, C., “Closed-form Buckling Analysis of Stiffened Composite Plates and Identification of Minimum Stiffener Requirements,” *International Journal of Engineering Science*, Vol. 46, No. 10, 2008, pp. 1011–1034.
- [50] Liu, Q., Jrad, M., Mulani, S. B., and Kapania, R. K., “Global/Local Optimization of Aircraft Wing Using Parallel Processing,” *AIAA Journal*, Vol. 54, No. 11, 2016, pp. 3338–3348.